Chinese Journal of Natural Medicines

Discovery and synthesis of 3–amino glycyrrhizin derivative containing guanidyl with anti–colorectal cancer activity

Jianrong Liu, Jingke Zhang, Tianbo Wu, Tingting Jin, Quanyi Zhao, Dian He

Citation: Jianrong Liu, Jingke Zhang, Tianbo Wu, Tingting Jin, Quanyi Zhao, Dian He, Discovery and synthesis of 3–amino glycyrrhizin derivative containing guanidyl with anti–colorectal cancer activity, Chinese Journal of Natural Medicines, 2026, 24(9), 1129–1145. doi: 10.1016/S1875–5364(26)61210–1.

View online: https://doi.org/10.1016/S1875–5364(26)61210–1

Related articles that may interest you

Diversity–oriented synthesis of marine sponge derived hyrtioreticulins and their anti–inflammatory activities

Chinese Journal of Natural Medicines. 2022, 20(1), 74–80 https://doi.org/10.1016/S1875–5364(22)60155–9

Synthesis and anti–HIV activities of phorbol derivatives

Chinese Journal of Natural Medicines. 2024, 22(2), 146–160 https://doi.org/10.1016/S1875–5364(24)60587–X

Synthesis, and anti–inflammatory activities of gentiopicroside derivatives

Chinese Journal of Natural Medicines. 2022, 20(4), 309–320 https://doi.org/10.1016/S1875–5364(22)60187–0

Potential of ginsenoside Rh_2 and its derivatives as anti–cancer agents

Chinese Journal of Natural Medicines. 2022, 20(12), 881–901 https://doi.org/10.1016/S1875–5364(22)60193–6

Seco–cyclic phorbol derivatives and their anti–HIV–1 activities

Chinese Journal of Natural Medicines. 2024, 22(4), 365–374 https://doi.org/10.1016/S1875–5364(24)60630–8

Chang Wei Qing Decoction enhances the anti–tumor effect of PD–1 inhibitor therapy by regulating the immune microenvironment and gut microbiota in colorectal cancer

Chinese Journal of Natural Medicines. 2023, 21(5), 333–345 https://doi.org/10.1016/S1875–5364(23)60451–0

Wechat

Chinese Journal of Natural Medicines 24 (2026) 1129-1145

Contents lists available at ScienceDirect

Chinese Journal of Natural Medicines

journal homepage: www.cjnmcpu.com/

Original article

Discovery and synthesis of 3-amino glycyrrhizin derivative containing guanidyl with anti-colorectal cancer activity

Jianrong Liu[a,Δ], Jingke Zhang[b,Δ], Tianbo Wu[a], Tingting Jin[a], Quanyi Zhao[a,*], Dian He[a]

[a] *Institute of Medicinal Chemistry, School of Pharmacy of Lanzhou University, Lanzhou 730000, China*
[b] *Medical Laboratory Center of Lanzhou University, Lanzhou 730000, China*

ARTICLE INFO

Article history:
Received 27 October 2025
Revised 26 February 2026
Accepted 3 March 2026
Available online 20 September 2026

Keywords:
GN-derivatives
HMGB1
Anti-cancer
Anti-inflammation

ABSTRACT

Colorectal cancer is considered to be a highly immune-related disease, and the severe chronic inflammatory stress in the tumor microenvironment (TME) greatly impedes the effective prognosis and treatment of colorectal cancer. Based on a dual strategy, anti-proliferation and inhibition of inflammatory factor HMGB1, a series of GN-derivatives were synthesized and screened for their anticancer efficacy, and compound **22** showed the strongest anti-proliferative activity against HCT116 cells, with IC_{50} value 13.1 μmol·L^{-1}. To improve the solubility, compounds **23**–**40** were synthesized and then evaluated for activities against colon cancer cells. Finally, compounds **23** and **24** with good water solubility were screened as target molecules. In anti-proliferation tests, both displayed the strongest activity on CT26 cells, with IC_{50} value 1.1 and 1.4 μmol·L^{-1}, respectively; in the cloning tests, they also showed a strong anti-proliferative activity against CT26 cells; moreover, they promoted apoptosis, and blocked cells in G_2/M phase in a concentration-dependent manner; in Western Blot tests, they decreased the levels of cyclin A2, cyclin B1 and CDK1 in a concentration-dependent manner. In anti-inflammation aspect, both them displayed strong anti-inflammation activity; compound **23** reduced the levels of NO in both RAW264.7 cells and CT26 cells in the anti-inflammatory tests, and the IC_{50} values were 10.3 and 1.1 μmol·L^{-1}, respectively; Western Blot showed **23** decreased the levels of HMGB1, RAGE, TNF-α, IL-6, IL-1 and COX-2 in a dose-dependent manner. In animal tests, compound **23** reduced the volume and weight of tumor more obviously than compound **24** and 5-FU, and its effect was a dose-dependent. In summary, compound **23** has therapeutic effect for the treatment of colorectal cancer in some degree, and it has potential to be a candidate for treatment of colorectal cancer.

1. Introduction

Colorectal cancer is one of the most common malignant tumors worldwide, and its incidence and mortality increases year by year [1-3]. Clinically, surgery, chemotherapy, and antibody therapy are applied to colorectal cancer. Chemotherapy is common and convenient, but almost the all drugs used have significant side effects and low tissue selectivity; that is to say, during the treatment, the drugs also cause significant toxic side effects to normal cells [4-6]. Moreover, colorectal cancer cells in the advanced stages often spread from the body cavity to the abdominal cavity to lead to multiple metastases, which makes it more difficult to treat because chemotherapy and antibody drugs cannot penetrate [7,8].

Colorectal cancer is considered to be a highly immune-related disease. In the tumor microenvironment (TME), the chronic inflammation stress persists and lots of inflammatory factors are released [9-11]. These inflammatory factors play an important role in the generation and development of colorectal cancer. They not only can promote tumor cell proliferation, matrix degradation and remodeling, angiogenesis and immune-suppression, but also promote tumor invasion and metastasis [12,13]. Among the factors, high mobility group protein B1 (HMGB1) is an important inflammatory factor in TME, and it plays a crucial role in inflammatory and immune responses by mediating the release of various inflammatory factors and chemokines [14]. HMGB1 acts as a damage-associated molecular pattern (DAMPs) or an early warning signal under stress conditions, and it can also form a complex with CXCL12 to induce cell migration. HMGB1 responds to early injury signals (such as ROS) during tissue damage, releasing earlier than other damage markers (DAMPs) [15,16]. HMGB1 has a relatively long half-life, enabling it to form large complexes with other molecules that stabilize its circulation. Especially, HMGB1 also plays an important role in tumor development and treatment. HMGB1 often overexpresses in many forms of cancer, and extracellular HMGB1 in the TME promotes tumor development by enhancing anti-apoptotic mechanisms, inflammatory response, and immune system evasion [17]. Hence, inhibiting HMGB1 mediated signaling pathway is beneficial for the treatment of cancer, and HMGB1 inhibitor possibly is a potential drug to colorectal cancer.

In recent years, GA derivatives (GA is aglucon of glycyrrhizin) were confirmed to inhibit the activity of HMGB1 in immune cells,

* Corresponding author.
E-mail address: zhaoqy@lzu.edu.cn (Q. Zhao)
Δ These authors contributed equally to this work.

https://doi.org/10.1016/S1875-5364(26)61210-1
Copyright © 2026, China Pharmaceutical University. Published by Elsevier B.V. All rights are reserved.

as well as in cancer cells [18]. HMGB1 is a marker of inflammation in TME, and its expression level is high in both immune cells and cancer cells. GA derivatives with *N*-glycosidic linkage bond were found to exhibit good anti-inflammatory activities, and they dose-dependently reduced the levels of IL-1β and TNF-α in RAW264.7 cells and HK-2 cells. Additionally, the compounds showed dose-dependent inhibitory effects on the levels of HMGB1, TLR4, NF-κB, P-NF-κB, and NLRP3 in HK-2 cells; in septic mice, they reduced serum IL-1β and TNF-α expression levels in a dose-dependent manner, and inhibiting HMGB1, NLRP3, p-NF-κB and Caspase-1 p20 protein levels, finally improving renal injury symptoms in septic mice [19]. GA derivatives containing disulfide bonds also were confirmed not only to reduce the expression of HMGB1, TLR4, IL-1β, TNF-α and TGF-β1 in RAW264.7 cells, but also inhibit the expression of TLR4, IL-1β, Col1 and α-SMA in non-small cell lung cancer A549 cells; in animal model, the compounds significantly reduced the state of lung inflammation and fibrosis caused by paraquat, and decreased the level of HMGB1 in mouse lung tissue [20]. This shows the GA derivatives with inhibiting HMGB1 bioactivity significantly have strong anti-inflammation activities in different kind cells, and have anticancer activity in some degree. However, as far as the GA derivatives as HMGB1 inhibitors we obtained is concerned, their anticancer activities are lower. Therefore, to find GA derivatives with good anti-colorectal cancer proliferative activity is our objective.

In last a few years, 3-amino-substituted GA (GN) which the hydroxyl group at C-3 position of GA replaced with amino group (-NH_2) was found to show a stronger anti-cancer activity than GA [21]. It can be predicted the amide derivatives of GN are more stable than GA ester derivatives. It is well known that the esterification of carboxyl group at C-30 of GA could enhance the anticancer activity, and among methyl ester, ethyl ester and benzyl ester at C-30, the benzyl ester displayed the best anti-tumor activity [22]; in addition, introducing soluble amino acid fragments at C-30 position, this not only enhance the solubility of the compounds, but also improve their pharmacokinetic properties [23]. We thought modification of GN at C-30 position just like GA will enhance GN anti-proliferative inhibition activity. The process of target compound discovery and optimization is shown in Scheme 1.

Therefore, in order to obtain the active compounds for anti-colorectal cancer with high efficiency and low toxicity based on HMGB1 as the target, GN was selected as start material, and 3-amino group (-NH_2) was modified with active organic acid, following C-30 position introducing amino acid to obtain a series of GN derivatives. Then, their anti-inflammatory and anti-tumor activities are evaluated *in vitro* and *in vivo*. By which, we hope to obtain a candidate of colorectal cancer and provide a material foundation and theoretical basis for its treatment.

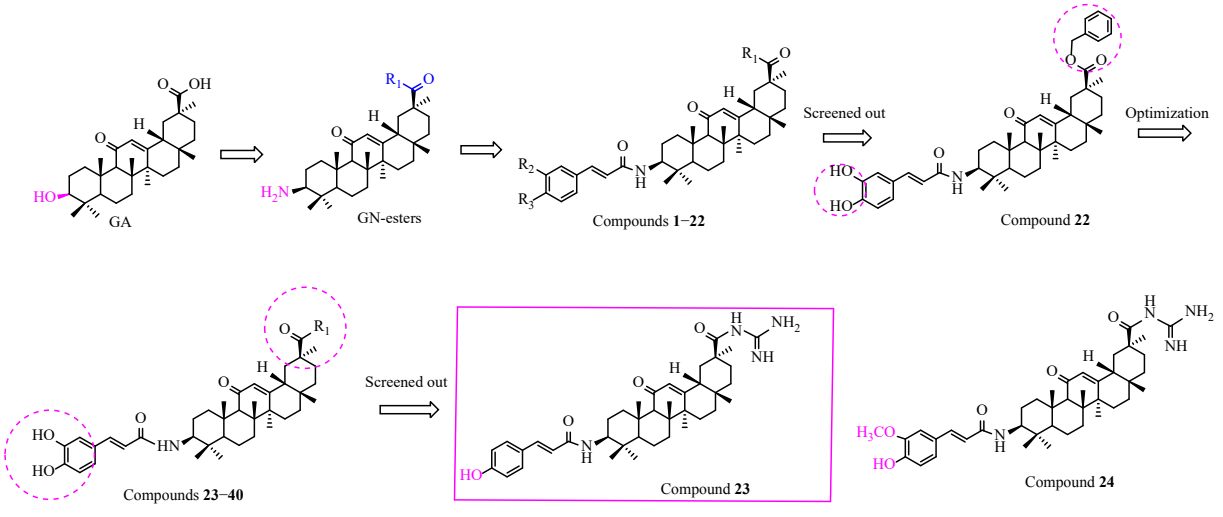
2. Results and discussion

2.1. Design, synthesis and characterization of compounds

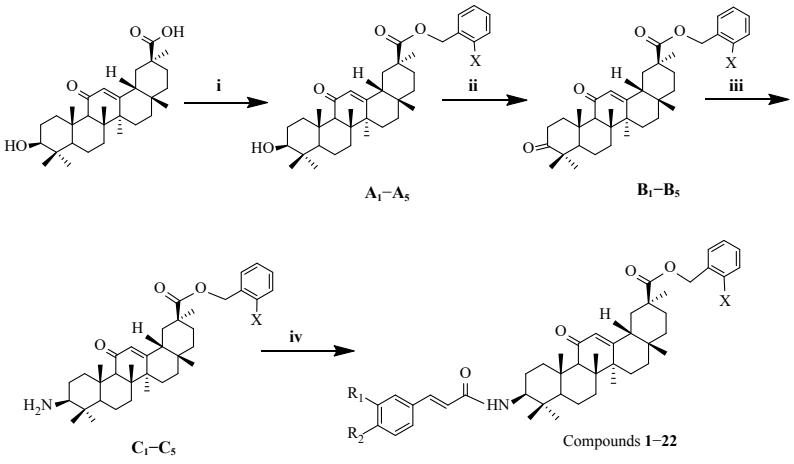
In the process of structural modification and optimization of compound, ester bond replacing with amide bond often improves its chemical properties and plasma metabolic stability, and even enhance the bio-activity of compound. The amide derivatives of GN are more stable than the ester derivatives of GA. The active organic acids including cassia bark acid, caffeic acid, and ferulic acid were chosen, because they are aromatic fatty acids with very low toxicity to the human body, and all have strong anti-inflammatory and anti-tumor properties [24, 25]. The *α* and *β*-unsaturated carbonyl groups in cassia bark acid are considered Michael acceptors, and cinnamic acid and its derivatives can effectively inhibit cancer cell proliferation, prevent cancer cell migration, and induce apoptosis. The combination of GN and active aromatic acid maybe exerts a positive synergistic anti-tumor effect [26, 27]. Therefore, to improve anticancer activity, benzyl or substituted benzyl groups were introduced at the C-30 position of GN, at the same time, cassia bark-acids or their derivatives were introduced at the C-3 position, resulting in compounds **1**–**20**. To further enhance the anti-tumor activity of these compounds, a hydroxyl group was added to the cassia bark-acid phenyl ring on basis of compound **1**. This change not only added the electron density of the phenyl ring but also facilitated hydrogen bonding with the target site, thereby enhancing the anticancer activity. Consequently, compounds **21**–**22** were synthesized.

The synthesis route and structure of compound **1**–**22** are illustrated in Scheme 2. Using GA as the starting material, it reacts with bromo-benzyl (or which has different substituents at the ortho position) in DMF to form glycyrrhizin benzyl ester. The OH group at C-3 position was then oxidized by PCC, and then reduced by $NaCNBH_3$ to form an important intermediate **C**. Finally, intermediate **C** was condensed with cassia bark-acid to yield compound **1**. The synthesis processes and workups for compounds **2**–**22** are similar to that of compound **1**.

In order to improve the solubility and biocompatibility of compounds, the carboxyl group at C-30 was transformed into amide by introducing amino acid or amino acid ester to obtain compounds **23**–**40**. The structure of compounds **23**–**40** and the synthesis process of compound **23** are shown in Scheme 3. Com-



Scheme 1 The whole idea and process of target compound discovery and optimization.



Scheme 2 Synthesis routes and structures of compounds **1**–**22**.

pound **23** was synthesized from GA, acylation, oxidation-reduction, and re-condensation with cassia bark acid derivative to amide, and finally deprotecting BOC under trifluoroacetic acid to obtain compound **23**. Compound **23** is good solubility. The synthesis and workups of other compounds **24**–**40** are similar to those of **23**.

In the synthesis process, the choice of oxidant is crucial in the oxidation of the hydroxyl group at C-3 position of GA to a ketone. Pyridine-chloroacetic acid (PCC) effectively oxidized secondary alcohols to ketones under mild conditions, with minimal side products and no over-oxidation. In contrast, other oxidants, such as 2-iodobenzoyl benzoic acid (IBX), can directly convert saturated alcohols into *α*, *β*-unsaturated carbonyl compounds and oxidize benzyl functional groups to phenyl ketones, resulting in more side products.

As for intermediate **C**, both two isomers (3*α*-NH_2 and 3*β*-NH_2) were obtained, but the product with 3*β* configuration was predominant and the yield was higher; moreover, they can be separated with column chromatography. In the condensation reaction process of forming the amide bond, the condensation agent is crucial factor; EDCI was good catalyst, the yield is higher; compared with EDCI, CDI showed a lower activity, and the yield is lower when it is used.

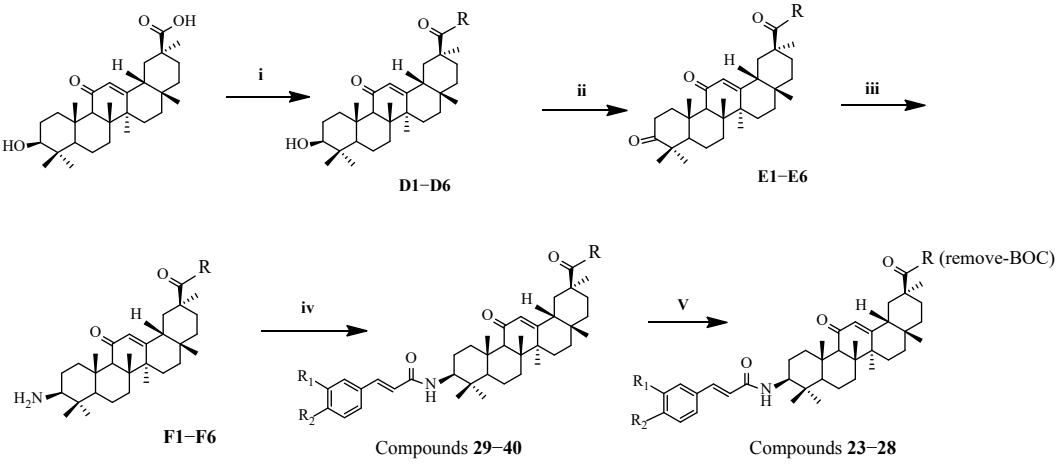
All the compounds were characterized by MS and NMR, and the spectral data of the compounds were consistent with expectations. In the infrared spectra, there are strong absorption peaks in the range of 1725–1735 cm^{-1}, which is the characteristic absorption of C=O in the ester group at C-30 in the five-ring skeleton. The absorption peak at about 1680 cm^{-1} is the characteristic absorption of C=O in the unsaturated ketone carbonyl at C-11 of GN. In the ^1H NMR spectra, the chemical shifts of CH-12 appear at about *δ* 5.6 as singlets, the chemical shifts of hydrogen atom in-OCH_3 at 30 appears at about *δ* 3.7 as singlets, and the signals of hydrogen atoms in CH_3-23, 24, 25, 26, 27, 28, 29 appear near *δ* 0.8–1.3 ppm as singlets. In the ^{13}C NMR spectra, the chemical shifts of the carbon atoms at the C-11 position of GA appeared around *δ* 200.3, the chemical shifts of the carbon atoms in the C=O group at the 30 position are around *δ* 177.1, the chemical shifts of the carbon atoms in the unsaturated double bonds at the C12 and C13 positions are near *δ* 128.7 and 169.4, respectively.

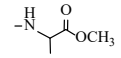
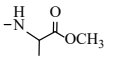
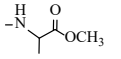
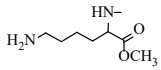
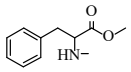
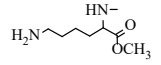
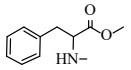
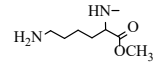
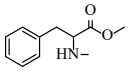
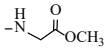
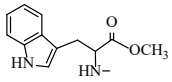
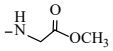
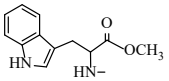
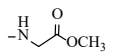
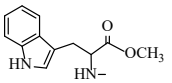
All compounds are white or light yellow solids at room temperature. Compounds **1**–**22** are highly soluble in common organic solvents such as dichloromethane, ethyl acetate, DMF, and DMSO, but they are insoluble in water, with a Clog *P* value of around 11. Compounds **23**–**28** are highly soluble in water, with a Clog *P* value ranging from 6.75 to 7.89. Compounds **29**–**40** have some water solubility, with a Clog *P* value ranging from 7.18 to 9.51 (Supplementary Table 1).

2.2. Anti-proliferative inhibition activities of compounds against cancer cells

In order to evaluate the inhibitory effect of the compounds on the proliferation of different cancer cells, CCK-8 method was used to determine the IC_{50} values of compounds **1**–**22** to six kinds of cancer cells with GA and 5-FU as positive controls [28]. As can be seen from Supplementary Table 2, most of the compounds showed very low anticancer activities against A549 and Hela cells, with IC_{50} values greater than 500 μmol·L^{-1}; for the three liver cancer cells, only compounds **16** and **19** showed slightly stronger activities against SK-HEP1 (IC_{50}, 25.1 ± 1.8 and 38.1 ± 1.5 μmol·L^{-1}), and the others displayed lower activities. However, most of the compounds showed good activities against colon cancer cell lines. Compounds **1**, **3**, **13**, **19**, **21** and **22** showed strong inhibitory effect on the proliferation of HCT116 cells; among them, compound **22** displayed the highest activity with IC_{50} value of 13.1 ± 1.7 μmol·L^{-1}. Seen from the IC_{50} values, the introduction of substituents on the benzene ring at C-30 of GN could not improve its anticancer activity, on the contrary, compound **1** without substituent on that showed high proliferative inhibition activity to HCT116 cells, and its IC_{50} value was 36.1 μmol·L^{-1}. However, the substituents of benzene ring on the cassia bark-acetic acid at C-3 of GN significantly influence activity. The OCH_3 group decreased the anti-proliferative inhibition activity on HCT116 cells (compound **2**, IC_{50}, 216.5 μmol·L^{-1}), and F atom enhanced the anti-proliferative inhibition activity (compound **3**, IC_{50}, 34.3 μmol·L^{-1}). However, when R_2 is NO_2, compound **4** showed a stronger activity than compound **2** (R_2 = OCH_3), but much lower than compounds **1** (R_2 = H) and **3** (R_2 = F). This indicates the effect of the substituent of cassia bark-acid on its anti-HCT116 activity is not significant. Unlikely, compounds **17**–**20** have obvious inhibitory activity against SK-HEP1 cells, and their IC_{50} is between 25.1–50 μmol·L^{-1}. There is a clear relationship between the structure and activity of compound. When the 4^{th} position of the benzene ring on cassia bark-acid (R_2) is substituted with -F, -NO_2, -H, and -OCH_3, the anti-hepatocellular carcinoma cell proliferation activity decreased progressively, with the order of activity F > NO_2 > H > OCH_3. This indicates that introducing electron-withdrawing groups on the benzene ring of cassia bark-acid is more beneficial for enhancing activity.

After introducing hydroxyl group on the cassia bark-acid, compounds **21** and **22** showed significant anti-proliferative inhibition against six types of cancer cells. Compound **21** exhibited superior inhibitory activity against HCT116 cells compared to compound **3**; and compound **22** showed strong anti-proliferative activity against various cell lines, especially in colorectal cancer, with IC_{50} of 13.1 μmol·L^{-1}. Markedly, two hydroxyl groups on the



Compounds	R	R_1	R_2	Compounds	R	R_1	R_2
23		**H**	**OH**	**32**		**H**	**OH**
24		**OCH_3**	**OH**	**33**		**OCH_3**	**OH**
25		**OH**	**OH**	**34**		**OH**	**OH**
26		**H**	**OH**	**35**		**H**	**OH**
27		**OCH_3**	**OH**	**36**		**OCH_3**	**OH**
28		**OH**	**OH**	**37**		**OH**	**OH**
29		**H**	**OH**	**38**		**H**	**OH**
30		**OCH_3**	**OH**	**39**		**OCH_3**	**OH**
31		**OH**	**OH**	**40**		**OH**	**OH**

Scheme 3 Synthesis routes and structures of compounds **23**–**40**.

aromatic ring of cassia bark-acid further intensified the inhibitory activity. This may be due to the hydroxyl group enhancing its affinity for the large target protein by forming hydrogen bonds.

Considering compounds **1**–**20** showed better activities against colorectal cancer and hepatocellular carcinoma cells than against A549 and Hela cells, compounds **23**–**40** were evaluated using colorectal cancer cells (HCT116, CT26 and HT-29) and hepatocellular carcinoma cells (SK-HEP1, HEPG2, Huh7). As can be seen from Supplementary Table 3, compounds **23**, **24**, **25**, **28**, **27**, **30**, **31** and **34** showed strong inhibitory effect on the proliferation of CT26 and HT-29 cells, and their IC_{50} values were all below 30 μmol·L^{-1}; among them, compounds **23** displayed the strongest proliferative inhibition on CT 26 cells, and **24** was the next; their IC_{50} values were 1.1 and 1.4 μmol·L^{-1} respectively. This indicates introducing polar groups or amino acids at the C-30 position of GN possibly enhanced inhibitory activities against colon cancer cell proliferation, and improved the selectivity against CT26 cells. Of these compounds, **23**–**25** have guanidine fragments at the C-30 position, and **26**–**28** have lysine fragments; both them are with a free amino group at the end. They not only have high water solubility but also strong anti-proliferative activity. Possibly, the polar groups were beneficial to the compound molecules to penetrate cell membranes. Compound **23** exhibited a higher inhibitory activity against CT26 cells than compound **28**, possibly due to its lower lipophilic-to-water partition coefficient (**23**, Clog *P* 6.75; **28**, Clog *P* 7.19). Significantly, compound **23** also displayed strong proliferative inhibition against three types of liver cancer cells, while **28** showed significant activity only for colon cancer, suggesting the longer amino acid carbon chain is

beneficial to enhance selectivity to colon cancer. The relationship of structure and activities (SAR) from compounds **29**–**40** indicates that smaller amino acid fragment (e.g. glycine and alanine) can enhance activity more significantly than the larger ones like phenylalanine and leucine. This is not only because the bio-activities are determined by their lipid-water partition coefficients and p*Ka*, but also the spatial steric hindrance between compound and target site is crucial factor. As shown in Supplementary Table 3, the substituents on the aromatic ring of cassia bark-acids also significantly influenced the proliferative inhibition of compounds. Of compounds **23**–**25**, compound **23** with one OH group exhibited the strongest activity, while compound **25** with two OH groups displayed a lower activity than **23**. This is possibly because the intramolecular hydrogen bonds formed by the two OH groups affected the compound's binding to target site. However, for compounds **26**–**28**, compound **28** with two OH groups on the cassia bark-acid benzene ring, exhibited higher activity than **26**. This is the opposite of the activity order observed in compounds **23**–**25**. This difference may be attributed to the elongation of the carbon chain at C-30 to enhance the molecule's lipophilicity. For these soluble compounds, the presence of two OH groups significantly affects binding to target sites or metal ions in active sites, thereby influencing anticancer activity. Therefore, we draw a conclusion that the introduction of amino acids at C-30 mainly affects the lipid-water partition coefficient, p*Ka* value and affinity to the target site, while the substituents on the cassia bark acid benzene ring mainly affect the binding to the target site. The relationships of structures of compounds and activities (SAR) are summed up as Scheme 4.

Based on the results of proliferative inhibition of cancer cells by all compounds, compounds **22**, **23**, **24**, **27** and **28** were selected as target molecules to carry out in follow-up tests.

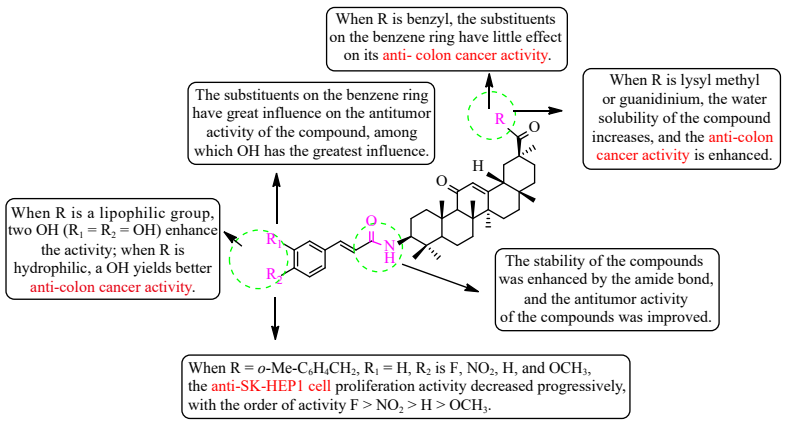
2.3. Effect of compound concentrations on colorectal cancer cells proliferation

In order to illustrate the inhibitory effect of the compounds on the proliferation of colorectal cancer cells, the HCT116 cells were treated with different concentrations of the compound for 24 h, then stained with DAPI/EdU, and then observed under the fluorescence microscope. DAPI (4',6-diamino-2-phenylindole) mainly stains the DNA in the nuclei, and it emits blue fluorescence under ultraviolet excitation by binding specifically to the AT base sequence in the double helix groove of DNA [29]. EdU (5-Ethynyl-2'-deoxyuridine) is a thymidine analog, which is incorporated into the newly synthesized DNA chain during cell DNA replication to form a stable mark, thus EDU mainly stains proliferating cells in the DNA synthesis period (S phase). The proliferative ability of cells was quantitatively evaluated by detecting the red fluorescence signal of the marker. In combination with EdU and DAPI, the nucleus was first labeled with DAPI (blue), and then the proliferating cells were labeled with EdU (emission wavelength 500–700 nm red/450–550 nm green light), so as to distinguish the proliferating cells from the total cell population through different fluorescence signals.

As shown in Fig. 1, in the control group, after EdU staining, the HCT116 cells showed strong red fluorescence, indicating most of the HCT116 cells were in the proliferative phase and the cell proliferation rate was fast; However, when the HCT116 cells were treated with GA (50 μmol·L^{-1} or 5-FU 50 μmol·L^{-1}) or compound **22**, the red fluorescence became gradually weak with concentration of the compound increasing. This indicates the anticancer activity of compound increased with the concentration and it is concentration-dependent. Compared with 5-FU or GA, compound **22** showed higher anti-proliferative inhibitory activities. When it was 25 μmol·L^{-1}, the positive rate of EdU cells decreased to about 10%, indicating only 10% HCT116 cells are alive. As for 5-FU and GA, when they are 50 μmol·L^{-1}, the positive rate of EdU cells decreased to about 43% and 35%, respectively. This suggests compound **22** had a higher inhibitory activity against HCT116 cells than the control 5-FU and GA.

Similarly, compound **23** exhibited effects on CT26 cell proliferation comparable to those observed in HCT116 cells. After 24 h co-culture with CT26, the green fluorescent protein (GFP) intensity gradually decreased, indicating Edu-positive cell ratios reduced in a dose-dependent manner. This demonstrates the anticancer activity of compound increased with concentration increase; and it outperformed both the control drugs GA and 5-FU. When compound **23** was 3 μmol·L^{-1}, the Edu-positive cell rate dropped to approximately 30% (Figs. 2A and 2B).

As a comprehensive indicator of cellular functional level, the formation rate of cloning can reflect the influence of compounds on long-term survival and proliferation ability of cells more comprehensively, which is an indispensable part of the evaluation system of compound biological properties. To further confirm the inhibition of compound **23** on the proliferation and invasiveness of CT26, the clonal formation of CT26 cells were investigated in the presence of compound **23**. Seen from the formation process of the blank group CT26 cell clone, the cell colony became larger and larger with the increase of time (Figs. 2C and 2D). This indicates CT26 cells easily form cloning, and they have a high probability of tumor formation *in vivo* (subsequent animal experiments, tumor models are made with CT26 cells). However, when compound **23** was co-incubated with the CT26 cells, the formation rate of clones significantly slowed down, and it was concentration-dependent (Fig. 2E). When compound **23** was 3 μmol·L^{-1}, the cell clonal formation almost inhibited completely, and the inhibitory rate reached nearly 100%. This indicates the compound possesses strong anti-CT26 cell proliferative and invasive capabilities.



Scheme 4 The relationships of structures of compounds and activities (SAR).

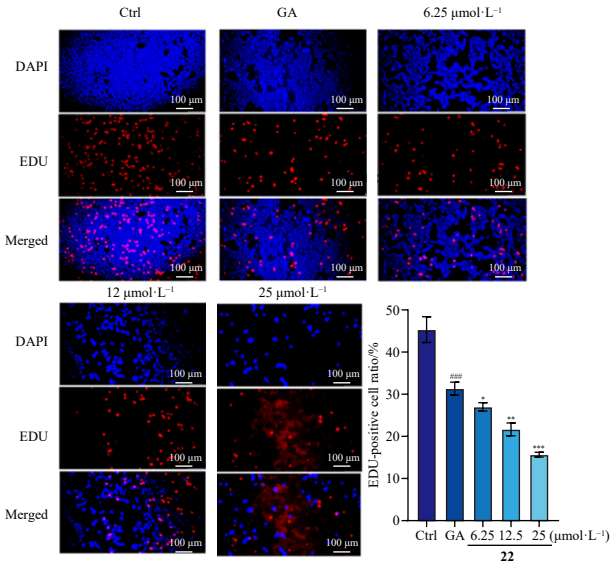


Fig. 1 EdU fluorescence intensity (emission wavelength 500–700 nm, magnification 20 × , scale = 100 μm) after exposure of cells to compound **22** and GA (25 μmol·L^{-1}) for 24 h (GA, positive control). Data are presented as mean ± SD (n = 3 independent tests). $^{*}P < 0.05$, $^{**}P < 0.01$, $^{***}P < 0.001$ indicate significant differences between the compound group and the GA group; $^{\#\#\#}P < 0.001$ indicates significant differences between the GA group and the blank control group.

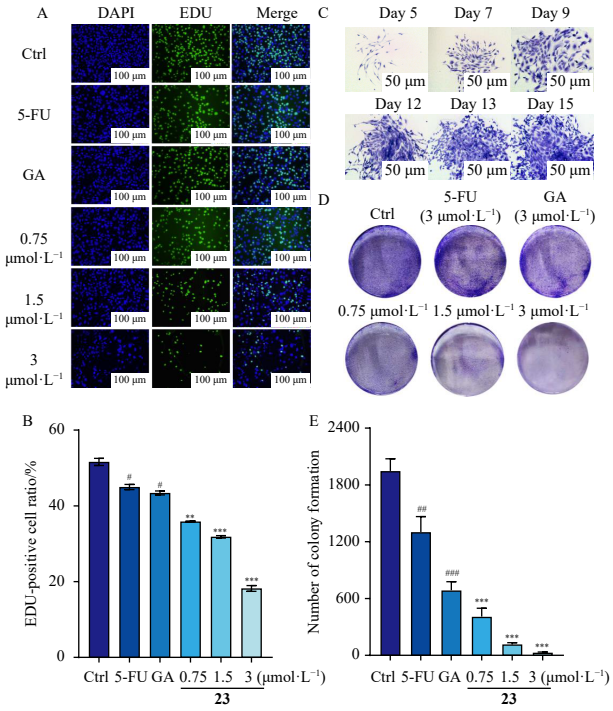


Fig. 2 (A, B) EdU fluorescence intensity after exposing cells to compound **23**, GA (3 μmol·L^{-1}), and 5-FU (3 μmol·L^{-1}) for 24 h (emission wavelength 450–550 nm, magnification 20 × , scale bar = 100 μm) (GA and 5-FU, positive control). (C) The formation process of CT26 cell clones in the control group (magnification 40 × , scale bar = 100 μm). (D) The clone clusters of CT26 cells treated with compound. (E) The statistical diagram of clone clusters of CT26 cells. Data are presented as mean ± SD (n = 3 independent tests). $^{*}P < 0.05$, $^{**}P < 0.01$, $^{***}P < 0.001$ indicate significant differences between the compound group and the GA group; $^{\#}P < 0.05$, $^{\#\#}P < 0.01$, $^{\#\#\#}P < 0.001$ indicates a significant difference between the GA group and the 5-FU group compared with the blank control group.

2.4. Effects of compounds on the cell cycle and the migration

The cell cycle consists of four stages: G_1 phase (cell growth and functional preparation), S phase (DNA replication), G_2 phase (cell growth and preparation for division) and M phase (cell division). The inhibition of the cell cycle of cancer cells is one of reasons to lead to the cell apoptosis, and it is positively correlated with the anticancer activity of compound.

In order to determine whether the compounds arrest the cell cycle, the HCT116 cells were treated with compound and stained with PI, and then analyzed by flow cytometer. As shown in Fig. 3 and Supplementary Fig. 1, after the HCT116 cells were treated with **22** for 24 h, the cells in the G_2/M phase significantly increased, while the cells in the G_0/G_1 phase decreased. In the control group, the proportion of in the G_2/M phase was 4.85%. As compound **22** increased, the cells in the G_2/M phase also rose. When **it** was 25 μmol·L^{-1}, the cells in the G_2/M phase increased to 20.43%, and the cells in the S phase decreased to 18.24%. This indicates the compounds blocked HCT116 cells in G_2/M phases in a concentration-dependent manner.

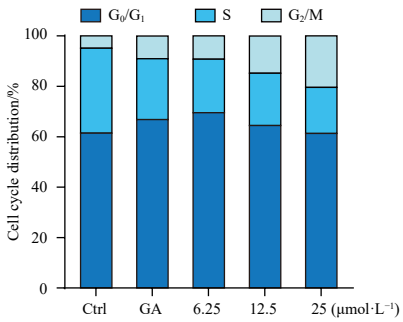


Fig. 3 Effects of different concentrations of compound **22** and GA (25 μmol·L^{-1}) on the cell cycle of HCT116 cells. Statistical analysis of cell cycle distribution percentages. Data are presented as mean ± SD (n = 3 independent tests).

In addition to cell HCT116, the compounds also arrested the cell cycle of CT26. After co-incubated with compound for 24 h, the proportion of cells in G_2/M phase also increased, while the proportion of cells in G_0/G_1 phase decreased. In the blank group (5-FU), the cells in G_2/M phase accounts for 4.85%. With the increase of compound concentration, the proportion of cells in G_2/M phase gradually increased, this is just like for HCT116 cells. Compared with 5-FU and GA, the compounds (**23**, **24**, **27** and **28**) all showed good activities. Among them, compound **23** displayed the strongest cell cycle arrest effect, and **24** was the next. When compound **23** was 3 μmol·L^{-1}, the cells in G_2/M phase increased to 20.43%, which were 8–10 folds as much as that of 5-FU and GA at the same concentration (Fig. 4 and Supplementary Fig. 2). This suggests that one of the reasons for the anti-tumor effect of compound was to block the cells in G_2/M phase in a dose-dependent manner, further giving rise to cell apoptosis.

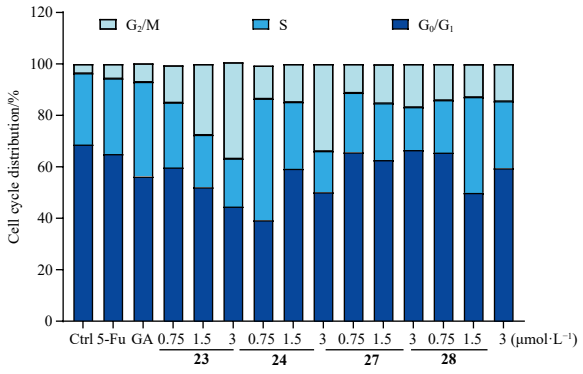


Fig. 4 Effects of different concentrations of compounds **23**, **24**, **27**, **28**, GA (3 μmol·L^{-1}), and 5-FU (3 μmol·L^{-1}) on the cell cycle of CT26 cells (GA and 5-FU, positive control). Data are presented as mean ± SD (n = 3 independent tests).

In the course of colorectal cancer development, cancer cells may break away from the primary tumor and enter the surrounding blood or lymphatic system, spreading to other parts of the

body through the blood or lymph fluid, forming metastatic tumors. To confirm whether the compounds inhibit the migration of colorectal cancer cells, a series of scratch tests were done. The results are shown in Fig. 5 and Supplementary Fig. 3. In the blank group, the scratch began to heal after 24 h, and by 72 h the healing rate of HCT116 cells was 81.26%, indicating significant cells migration without compound. However, when the cells treated with the compound, the cell healing rate decreased, and it decreased with compound increasing. When compound **22** was 6.25 μmol·L^{-1}, the cell migration rate of HCT116 cells was 30.42% for 24 h; and when it was 12.5 μmol·L^{-1}, the cell migration rate was only 18.74%. This indicates the compound inhibited the migration of HCT116 cells in a concentration-dependent manner.

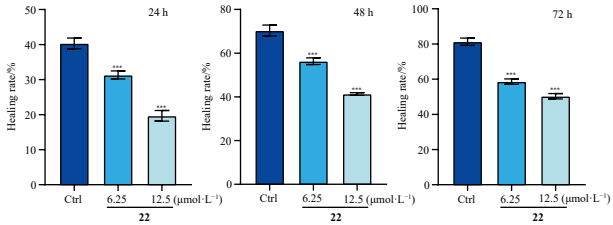


Fig. 5 Effect of compound **22** at different concentrations on the migration of HCT116 cells. Data are presented as mean ± SD (n = 3 independent tests). $^{*}P$ < 0.05, $^{**}P$ < 0.01, $^{***}P$ < 0.001 *vs* the control group.

Similarly, the tested compounds also strongly inhibited the migration of CT26 cells. Seen from Fig. 6 and Supplementary Fig.4, in the control group (5-FU), the wounds began to heal after 24 h, in the subsequent 48 h period, the wound areas showed significant cell migration, with a healing rate of 81.26%. After being treated with compounds **23**, **24**, **27**, and **28**, compared to 5-fluorouracil (5-FU) and GA, the cell migration rates significantly decreased, this indicates all the compounds have a strong inhibition on the migration of CT26 cells. Among them, compound **23** showed the highest activity. As the concentration of compound **23** increased, the cell migration rate decreased in a dose-dependent manner. When it was 1.5 μmol·L^{-1}, the cell migration rate of CT26 cells was only 18.74% after 24 h, and the cell healing rate was below 50% after 48 h. This indicates the compounds also inhibited CT26 cells migration, and decreased the cell healing rate. Therefore, we draw a conclusion that the compounds can inhibit colorectal cancer cells migration, and it is concentration-dependent.

2.5. Effect of compound concentration on apoptosis of CT26 cells

To induce cell apoptosis is one of the mechanisms of anticancer for compound, and the cell numbers of apoptosis is correlated with its anti-tumor activity. When CT26 cells were co-incubated with compound for 24 h and then stained with Giemsa [30]. Under an optical microscope, some cells were shrinkage and cytoplasm condensation, and some cell nuclei fragmented into nuclear debris, indicating the formation of apoptotic bodies (Fig. 7). With the concentration of compound increasing, more apoptotic bodies formed; while the CT26 cells in the control group did not show the significant signs of apoptosis. Compared with 5-FU and GA, compounds **23**, **24**, **27** and **28** showed strong pro-apoptotic effects.

To further confirm the promotion of the compounds on apoptosis of CT26 cells, the apoptosis were analyzed by flow cytometer.

Seen from Fig. 8 and Supplementary Fig. 5, all the tested compounds induced the CT26 cells apoptosis, and the effects were concentration-dependent. Compared with 5-FU and GA, the compounds showed stronger activities to induce apoptosis. For **23**, **24**, **27** and **28**, they mainly induced CT26 cells early apoptosis. When **24** was 0.75, 1.5 and 3 μmol·L^{-1} respectively, the proportions of early apoptosis rates account for 10.91%, 21.96% and 34.37%, respectively; for compound **27** under the same concentration, the early apoptosis rates increased from 3.62% to 7.28%, 9.84% and 33.77%, respectively. for compound **27**, the early apoptosis rates increased from 3.62% to 7.28%, 9.84% and 33.77%, respectively. as for compound **28**, the early apoptosis rates are 5.57%, 32.96%, and 35.45% respectively, showing obvious concentration dependence. However, unlike the three compounds above, compound **23** significantly promoted both early and late apoptosis. When it was 0.75 μmol·L^{-1}, the proportion of early apoptosis accounts 27.79%, and the proportion of late apoptosis was 30.29%; the total apoptosis rate was 46.27%; when it was 1.5 μmol·L^{-1}, the early apoptosis rate was 31.03%, the late apoptosis rate 30.29%; and the total apoptosis rate was 61.32%; when it was up to 3 μmol·L^{-1}, the early apoptosis rate increased to 43.85%, the late apoptosis rate increased to 33.13%, and the total apoptosis rate arrived in 76.98%.

In contrast, compound **23** showed stronger activity to induce CT26 cell apoptosis, which is consistent with its inhibitory effect on cell proliferation. This also suggests induction of apoptosis in a dose-dependent manner is one of the reasons for compound to inhibit tumor cell proliferation.

To deeply understand the process of apoptosis, the CT26 cells were stained with a combination of Hoechst 33342 and PI. As shown in Fig. 9, with the increase of the concentration of compounds **23**, **24**, **27** and **28**, the blue fluorescence becomes stronger, which is because the change of cell membrane permeability of apoptotic cells, leading to the increased uptake of Hoechst 33342 dye [31]; At the same time, as the concentration increased, the red fluorescence became stronger, indicating an in-

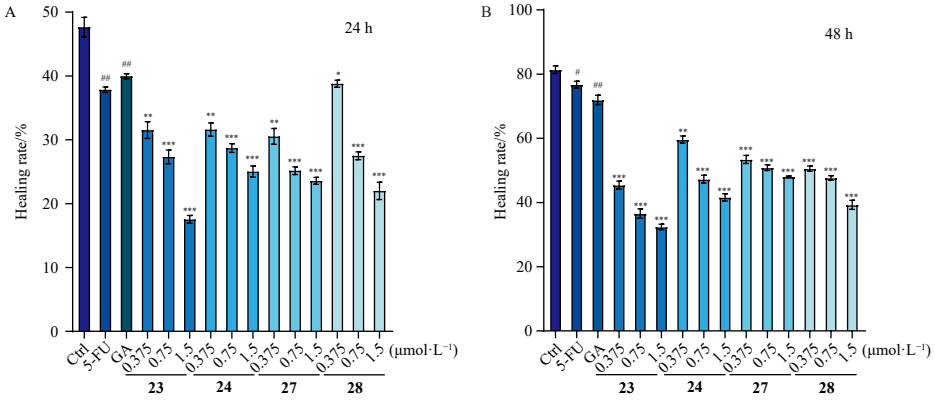


Fig. 6 Effects of the compounds, GA (3 μmol·L^{-1}), and 5-FU (3 μmol·L^{-1}) on CT26 cell migration. The statistical graphs of the migration of CT26 cells treated with compounds **23**, **24**, **27**, and **28**, as well as GA (3 μmol·L^{-1}) and 5-FU (3 μmol·L^{-1}) for 24 h (A) and 48 h (B) respectively. Data are presented as mean ± SD (n = 3 independent tests). $^{*}P$ < 0.05, $^{**}P$ < 0.01, $^{***}P$ < 0.001 *vs* the GA group; $^{\#}P$ < 0.05, $^{\#\#}P$ < 0.01, $^{\#\#\#}P$ < 0.001 *vs* the blank control group.

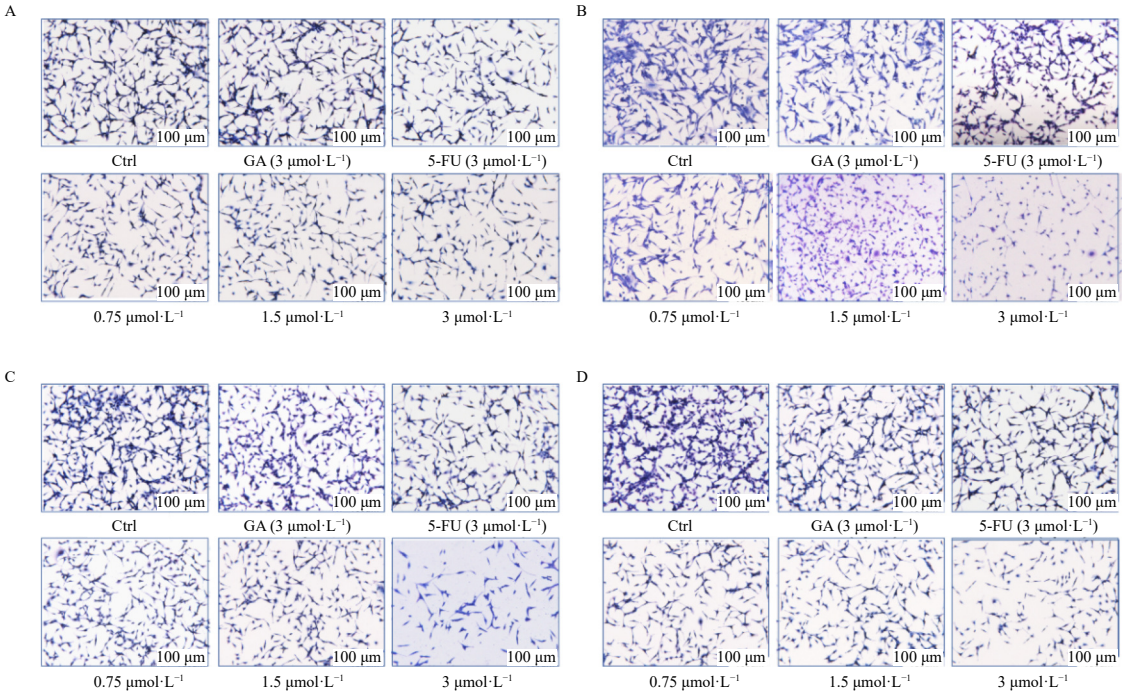


Fig. 7 Effects of different concentrations of the compounds, GA (3 μmol·L^{-1}), and 5-FU (3 μmol·L^{-1}) on the morphology of CT26 cells (magnification 20× , scale bar = 100 μm) (GA and 5-FU, positive control). (A) Stands for the blank control, GA (3 μmol·L^{-1}), and 5-FU (3 μmol·L^{-1}). (B) for **23**; (C) for **24**, (D) **27**, and (E) for **28**.

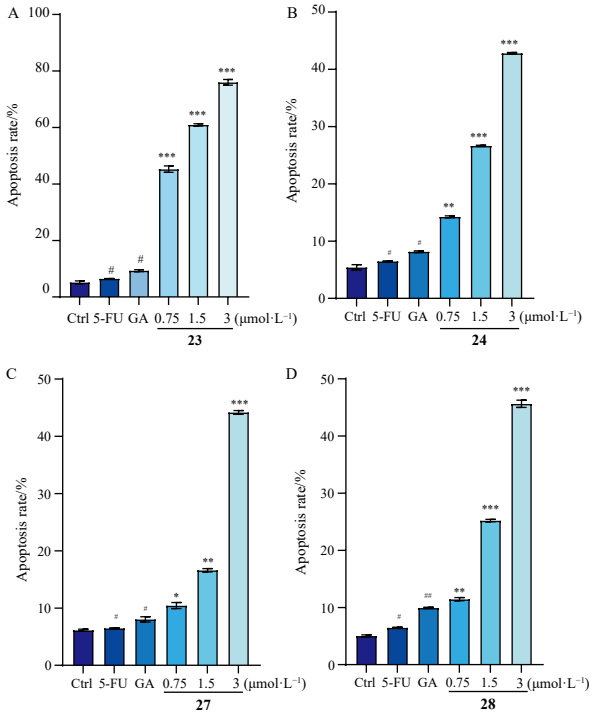


Fig. 8 Effects of different concentrations of compounds **23** (A), **24** (B), **27** (C), **28** (D) and GA (3 μmol·L^{-1}) and 5-FU (3 μmol·L^{-1}) on apoptosis in CT26 cells (GA and 5-FU, positive control). Data are presented as mean ± SD (n = 3 independent tests). $^{*}P < 0.05$, $^{**}P < 0.01$, $^{***}P < 0.001$ *vs* the GA group; $^{\#}P < 0.05$, $^{\#\#}P < 0.01$, $^{\#\#\#}P < 0.001$ *vs* the blank control group.

crease in necrotic cells. This indicates that the compounds induce apoptosis and necrosis of CT26 cells in a concentration-dependent manner.

2.6. Effect of compound concentration on ROS and MMP in CT26 cells

Under normal conditions, the mitochondrial membrane potential (MMP) maintains at a constant level to ensure mitochondrial function and cell survival [32]. As the center of the cell energy, mitochondria also play a role in regulating apoptosis. A decrease in MMP triggers the release of apoptotic factors, such as cytochrome c. To confirm whether the cell apoptosis induced by the compounds is achieved through the mitochondrial pathway, tetramethyl rhodamine ethyl ester (TMRE) was selected as a fluorescent probe to monitor changes in the MMP of CT26 cells. TMRE is a unique positively charged fluorescent probe specifically designed for studying MMP. It penetrates the cell membrane and accumulates within the inner mitochondrial membrane. In normal cells, the high MMP leads to significant dye accumulation, emitting strong red fluorescence; however, when the MMP decreases, the fluorescence intensity diminishes.

Seen from Fig. 10 and Supplementary Fig. 6, after co-incubation of the compound with CT26 cells for 24 h, the fluorescence intensity in all the treated cells was significantly reduced, and it gradually decreased with the concentration of compound increasing, this indicates the MMP in CT26 cells decreased in a concentration-dependent manner. When compound **23** was 0.75, 1.5 and 3 μmol·L^{-1}, the fluorescence intensity decreased from 98.83% to 79.77%, 59.67% and 18.19% of the blank control group, respectively; for **24**, it decreased from 98.55% to 83.87%, 71.10% and 59.17% under the same concentration; as for **27**, it decreased from 98.65% to 80.13%, 67.71% and 62.65%. for **28**, it decreased from 97.09% to 80.68%, 79.53% and 77.40%. This suggests that all the compounds reduced MMP in a concentration-dependent manner, further promoting tumor cell apoptosis. In contrast, compound **23** has higher activity to reduce MMP. This suggests the reduction of MMP is one of the internal reasons for the promotion of cell apoptosis by the compounds.

It is well known that when the MMP decreases, it may affect the ions balance inside and outside the mitochondria, resulting in the influence of the REDOX process inside the mitochondria. This abnormal REDOX state may lead to the production of excessive reactive oxygen species (ROS) [33]. In order to confirm this point, DCFH-DA was selected as the fluorescent probe and measured the ROS level in CT26 cells after treatment with the compound by flow cytometer.

The results are shown in Fig. 11 and Supplementary Fig. 7. Compared with the control 5-FU and GA groups, the level of ROS

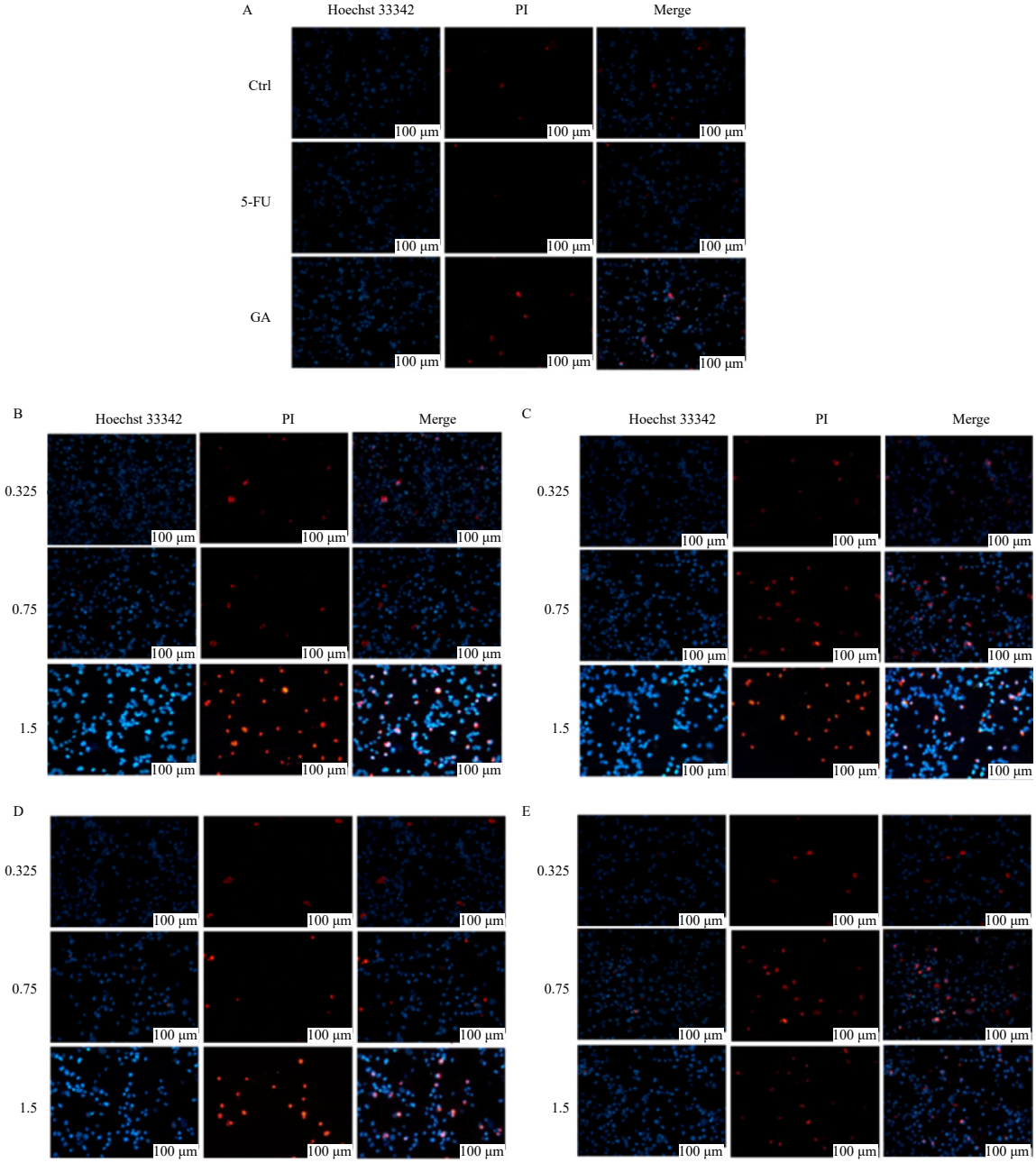


Fig. 9 Fluorescence images of CT26 cells stained with Hoechst 33342/PI at different concentrations of the compounds, GA (3 μmol·L^{-1}), and 5-FU (3 μmol·L^{-1}) (magnification 20× , scale bar = 100 μm) (GA and 5-FU, positive control). (A) is for the blank control, GA (3 μmol·L^{-1}), and 5-FU (3 μmol·L^{-1}). (B–E) are for compounds **23**, **24**, **27**, and **28** respectively.

in cells in compound group was significantly increased after the CT26 cells treated with compound for 24 h, and it was concentration-dependent. In contrast, compound **23** increased the level of ROS in CT26 cells more significantly than other tested compounds. This is consistent with their antitumor activities.

In conclusion, we can say the compounds inhibited colorectal cancer cells proliferation by reducing MMP and increasing the level of ROS, blocking the cell cycle, and further promoted the cells apoptosis, even necrosis.

2.7. Effects of compounds on biomarkers in CT26 cells

2.7.1. Effect of compound on apoptosis-related proteins and cycle-related proteins

Inhibiting signaling pathways in tumor cells often leads to changes in the expression of apoptosis-related proteins Bcl-2, Bax, Cyt-c and MMP9 [34]. As shown in Fig. 12 (12A, 12C–12G), compound **23** downregulated the expression level of the anti-apoptotic protein Bcl-2 and upregulated the level of the pro-apoptotic protein Bax, and the relative ratio of Bax and Bcl-2 increased with the concentration of compound **23** increasing; when **23** was 3 μmol·L^{-1}, it is up to about 1.2. Meanwhile, compound **23** inhibited the expression of MMP9 in a concentration-dependent manner; and induced Cyt-c release, which is a mitochondrial extracellular matrix protein.

In addition, compounds blocking CT26 cells in G_2/M phase must be give rise to the change of proteins about cell cycle. To explain this problem, the levels of cyclin B1, CDK1 and cyclin A2 were analyzed by Western Blot. As shown in Fig. 12 (12B, 12H–12J) the expression levels of cyclin B1 and CDK1 decreased in a concentration-dependent manner, indicating **23** inhibited the activities of the kinases required for the transition from G_2/M phase in the cell cycle; meanwhile, the expression level of cyclin

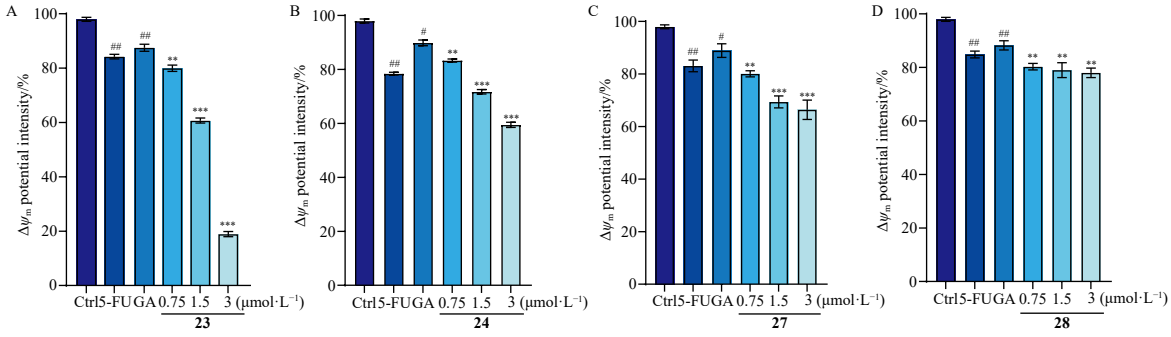


Fig. 10 Effects of different concentrations of the compounds **23** (A), **24** (B), **27** (C), **28** (D), GA (3 μmol·L^{-1}) and 5-FU (3 μmol·L^{-1}) on the mitochondrial membrane potential of CT26 cells (GA and 5-FU, positive control).Data are presented as mean ± SD (n = 3 independent tests). $^{*}P < 0.05$, $^{**}P < 0.01$, $^{***}P < 0.001$ *vs* the GA group; $^{\#}P < 0.05$, $^{\#\#}P < 0.01$, $^{\#\#\#}P < 0.001$ *vs* the blank control group.

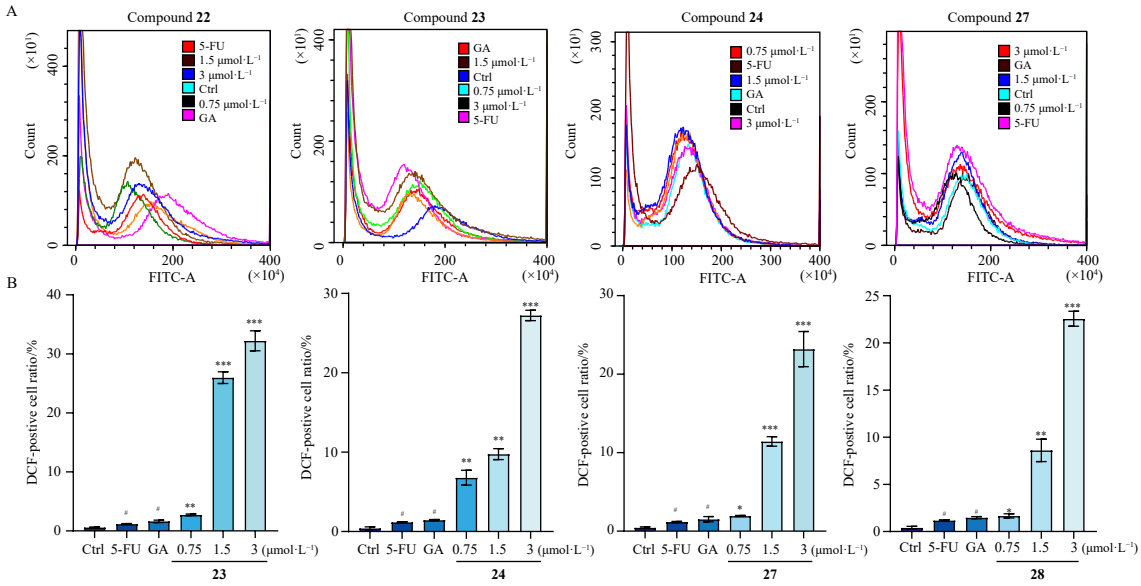


Fig. 11 Effects of different concentrations of the compounds **23**, **24**, **27**, **28**, and GA (3 μmol·L^{-1}) as well as 5-FU (3 μmol·L^{-1}) on reactive oxygen species (ROS) levels in CT26 cells (GA and 5-FU, positive control). Data are presented as mean ± SD (n = 3 independent tests). $^{*}P < 0.05$, $^{**}P < 0.01$, $^{***}P < 0.001$ *vs* the GA group; $^{\#}P < 0.05$, $^{\#\#}P < 0.01$, $^{\#\#\#}P < 0.001$ *vs* the blank control group.

A2 also downregulated gradually with the concentration increasing, suggesting that compound **23** may simultaneously affect the progression from S phase to G_2 phase, leading to cell arrest at the G_2/M phase.

2.8. Anti-inflammatory activity of compounds

2.8.1. NO inhibition of compounds on RAW264.7 cells and colon cancer cells

Whether the compounds maintain anti-inflammation within microenvironment of tumor is another key question to our research. To evaluate the anti-inflammatory activities of the compounds (**23**, **24**, **27**, and **28**), LPS-induced RAW264.7 cells, or HCT116 or CT26 cells were used as a model. In the tests, the content of NO in cells induced by LPS was defined as the maximum value, and the anti-inflammatory activity of the compound was evaluated by calculating the inhibition rate of NO release. After treated the RAW264.7 cells with compound for 24 h, the content of NO in RAW264.7 cells was measured by Greiss method (the survival rate of cells after LPS stimulation and compound intervention was not significantly reduced before the experiment).

In general, RAW264.7 cells are clearly rounded or oval in shape, and their morphologies change obviously after LPS stimulation. To visually observe morphological change, the LPS-stimulated RAW264.7 cells were stained with Giemsa and observed under microscope. Compared with the control group, the cells exhibited pseudopodia formation, transformed into spindle-shaped or polygonal forms with significant volume expansion. The cytoplasm showed a uniformly light purple coloration, while lysosomes and vacuoles increased in number. Notably, the nuclei became more prominent (Fig. 13). To reduce the deviation of anti-inflammatory results caused by cytotoxicity due to improper concentration, CCK-8 method was used to determine the half inhibitory concentration (IC_{50}) of compounds on RAW 264.7 cells (Table 1).

Then, the NO inhibitory tests of the compounds were carried out, and the NO inhibition IC_{50} values are shown in Table 2. As shown in Table 2, for both RAW264.7 cells and HCT116/CT26 cells, four compounds all demonstrated strong NO produce inhibition. This indicates the compounds not only inhibited tumor cell proliferation, but also exhibited anti-inflammatory activities within the tumor microenvironment. Their IC_{50} values are closely aligned with the cell half-inhibitory concentration (Supplementary Table 1), suggesting that the minimum concentrations of compounds for exerting the strongest anticancer and anti-inflammatory activities are close. Among the four compounds, compound **23** showed the strongest inhibitory activity to NO produce in three kinds of cell lines, and its IC_{50} values were 10.3, 20.1 and 1.1 μmol·L^{-1} respectively. So, the following tests mainly focused on compound **23**.

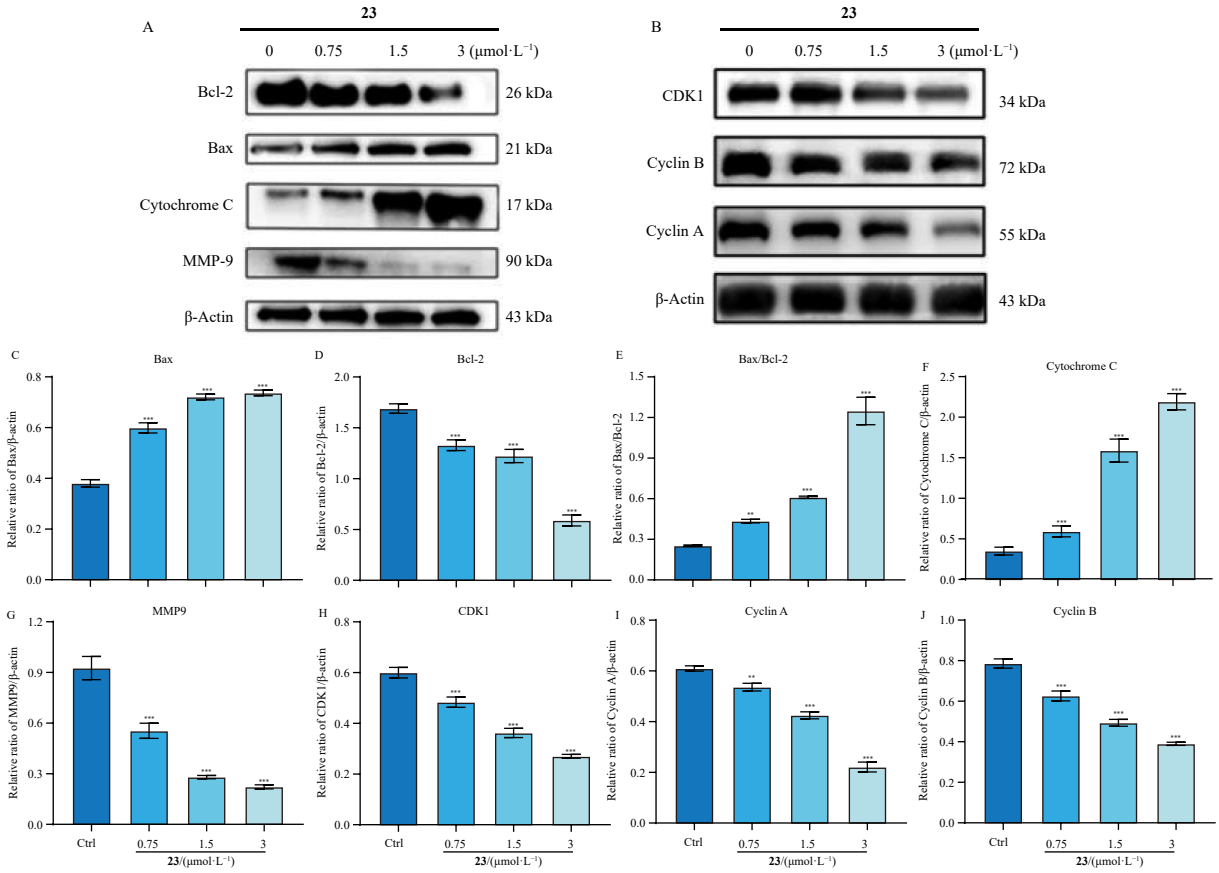


Fig. 12 Effects of compound on some biomarkers. (A) and (B) are the results of Western blotting, with β-actin as the internal control; (C–G) The relative levels of Bax, Bcl-2, Bax/Bcl-2, Cytochrome C, and MM9 proteins; (H–J) The relative levels of CDK1, Cyclin A, and Cyclin B proteins. Data are presented as mean ± SD (n = 3 independent tests). $^{*}P < 0.05$, $^{**}P < 0.01$, and $^{***}P < 0.001$ *vs* the blank control group.

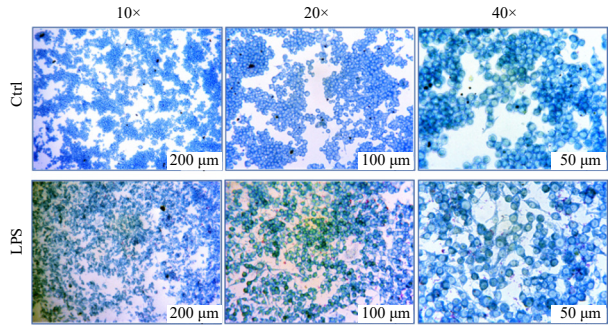


Fig. 13 Morphological changes in RAW264.7 cells after treatment with LPS (2 μg·mL^{-1}) for 24 h (Giemsa staining, magnification 10× , 20× , 40× , scale bars: 200 μm, 100 μm, 50 μm).

2.8.2. Effects of compounds on ROS and MMP in LPS-treated RAW264.7 cells

Reactive oxygen species (ROS) are byproducts of normal cellular metabolism. They also serve as key signaling molecules playing a crucial role in the development of inflammatory diseases. When oxidative stress occurs, excess ROS can attack proteins, lipids, and DNA within cells, leading to cellular damage. These damaged cells are cleared by the body, triggering the production of endogenous injury-related molecular patterns and the release of cytokines. To accesses the inhibitory effect of compounds on ROS induced inflammation, LPS-induced RAW264.7 cells were used as a model and co-cultured with compound **23** and **24** for 24 h, and then detected the level of ROS with DCFH-DA probe. As shown in the Fig. 14 and Supplementary Fig. 7, LPS stimulation significantly elevated intracellular ROS levels in RAW264.7 cells. However, when the cells treated with compound **23** or **24** at concentrations of 0.75, 1.5, and 3 μmol·L^{-1}, the cellular fluorescence intensity progressively decreased, indicating that ROS levels decrease with increasing compound concentration. When compound **23** was 3 μmol·L^{-1}, the ROS levels decreased to 9.3% of the LPS group; for **24**, the ROS levels decreased to 71.6% of the LPS group. In contrast, for GA at the same concentration, the ROS levels decreased to 85.1% of that. This demonstrates compound **23** exhibited much stronger anti-ROS activity than compound **24** and GA.

Under oxidative stress conditions, ROS may disrupt mitochondrial membrane structure and functionality, leading to a decrease in MMP. MMP is a crucial parameter for maintaining normal mitochondrial function. This reduction in MMP inevitably results in decreased ATP production within cells, causing energy deficiency that adversely affects cellular functions and survival. To further illustrate the effect of compound on MMP, the LPS

Table 1 IC_{50} values of compounds against three cell lines (Values represent the mean ± SD values of at least three independent tests).

Compds	IC_{50}/(μmol·L^{-1})			Compds	IC_{50}/(μmol·L^{-1})		
	RAW264.7	HCT116	CT26		RAW264.7	HCT116	CT26
23	13.6 ± 0.8	23.1 ± 1.4	1.1 ± 0.6	**24**	11.3 ± 1.4	33.4 ± 1.8	1.4 ± 1.2
27	12.9 ± 1.9	192.7 ± 5.4	15.2 ± 1.4	**28**	15.4 ± 0.3	320.4 ± 6.5	13.5 ± 1.5

Table 2 NO inhibition IC_{50} values of compounds in the LPS stimulation cells. (Values represent the mean ± SD values of at least three independent tests).

Compds	IC_{50}/(μmol·L^{-1})			Compds	IC_{50}/(μmol·L^{-1})		
	RAW264.7	HCT116	CT26		RAW264.7	HCT116	CT26
23	10.3 ± 1.8	20.1 ± 1.2	1.1 ± 0.8	**24**	13.9 ± 1.4	30.2 ± 1.2	1.3 ± 1.7
27	26.9 ± 1.9	80.3 ± 2.1	16.4 ± 1.9	**28**	17.2 ± 0.6	24.3 ± 1.6	18.1 ± 0.7

Note: IC_{50} represents the concentration of compound that inhibits 50% of NO produce in the LPS model group.

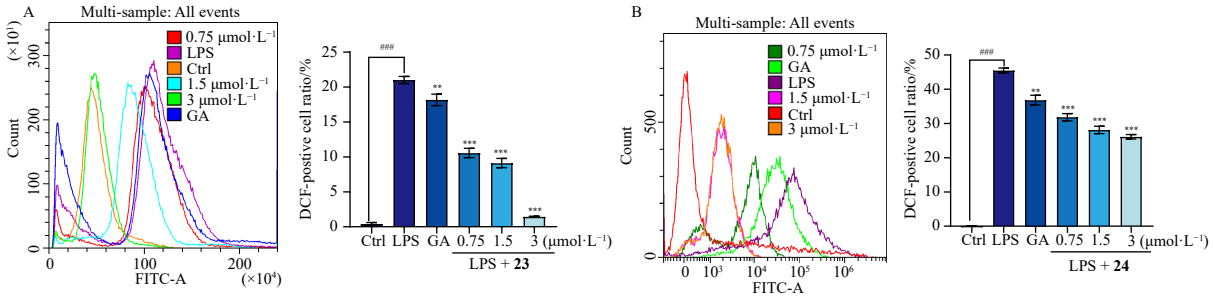


Fig. 14 Effect of compound **23** (A) and **24** (B) at different concentrations on ROS in LPS-induced RAW264.7 cells (GA, positive control). Data are presented as mean ± SD (n = 3 independent tests). $^{*}P < 0.05$, $^{**}P < 0.01$, $^{***}P < 0.001$ *vs* the LPS group; $^{\#\#\#}P < 0.001$ *vs* the blank control group.

treated RAW264.7 cells were used and the intracellular MMP levels were measured by flow cytometry using TMRE as the fluorescent probe.

As shown in Fig. 15 and Supplementary Fig. 8, LPS treatment resulted in a marked decrease in MMP levels in RAW264.7 cells. However, when compound **23** or **24** was co-incubated with these cells for 24 h, MMP levels significantly increased. As compound concentrations increased, MMP levels continued to rise. At a 3 μmol·L^{-1} concentration of compound **23**, levels approached the control; for **24**, MMP levels increased to 85% of the control group. This indicates that compounds **23** and **24** not only inhibit NO production but also effectively suppress the amplification and persistence of inflammatory responses by reducing intracellular reactive oxygen species (ROS) levels and enhancing MMP activity.

However, it is interesting to note that in the previous anti-RAW264.7 cell proliferation experiment, compounds **23** and **24** increased ROS and decreased MMP, but in the anti-inflammatory experiment using LPS- induced RAW264.7 cells as models, both them decreased ROS and increased MMP. This seems to be contradictory. In fact, this is reasonable. Because in tumor cells, ROS not only induces cells apoptosis, but also stimulates inflammatory responses. In LPS-induced RAW264.7 cells, the inflammatory stress is closely similar to that in tumor microenvironments; and the role of ROS as an inflammatory mediator far outweighs its function in inducing apoptosis.

2.8.3. Effect of compound on inflammatory factors in RAW264.7 cells

In colorectal cancer, beyond NO and ROS factors, the HMGB1/TLR4/NF-κB pathway plays a central role in inflammatory activation, and blocking this signaling pathway can mitigate NF-κB-mediated inflammatory responses. We first examined the effects of compounds **23** and **24** on HMGB1 and TLR4 protein expression levels. Western blot results showed that compared to the control group, LPS-treated RAW264.7 cells exhibited significantly elevated levels of TLR4 and HMGB1 proteins [35]. However, after treatment with compound **23** or **24**, both TLR4 and HMGB1 levels decreased in a concentration-dependent manner. At a compound concentration of 3 μmol·L^{-1}, compound **23** reduced TLR4 and HMGB1 levels to 27% and 41% of the LPS group, respectively; compound **24** reduced TLR4 and HMGB1 levels to 36% and 48% of the LPS group, respectively. Concurrently, the effects of compound **23** on downstream-associated proteins were examined, and the results demonstrated NF-κB p65 phosphorylation, along with TNF-α, IL-6, IL-1, and COX-2 levels were also reduced in a concentration-dependent manner (Fig. 16).

In general, abnormal activation of the HMGB1/RAGE pathway is associated with tumor progression, metastasis and treatment resistance. The binding of HMGB1 to RAGE activates the NF-κB, MAPK and PI3K/AKT pathways, promoting tumor cell proliferation, metastasis, angiogenesis and immune escape [36]. To illustrate the inhibition of the compound on the HMGB1/RAGE pathway, ELISA kit and WB were used to detect the expression levels of HMGB1 and RAGE in CT26 cells after treatment with compound **23** or **24** for 24 h. The results are shown in Fig. 17. Compared with the blank group, HMGB1 and RAGE protein expression levels decreased in a concentration-dependent manner. At the same time, compound **23** downregulated the PI3K/AKT path-

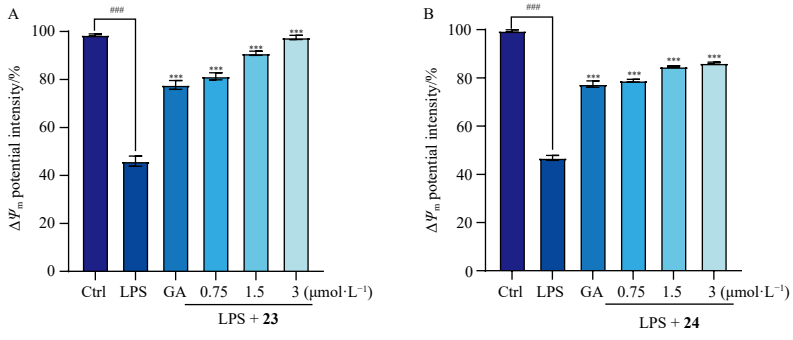


Fig. 15 Effect of compounds **23** (A) and **24** (B) at different concentrations on MMP in LPS-induced RAW264.7 cells (GA, positive control).Data are presented as mean ± SD (n = 3 independent tests). $^{*}P < 0.05$, $^{**}P < 0.01$, $^{***}P < 0.001$ *vs* the LPS group; $^{\#\#\#}P < 0.001$ *vs* the blank control group.

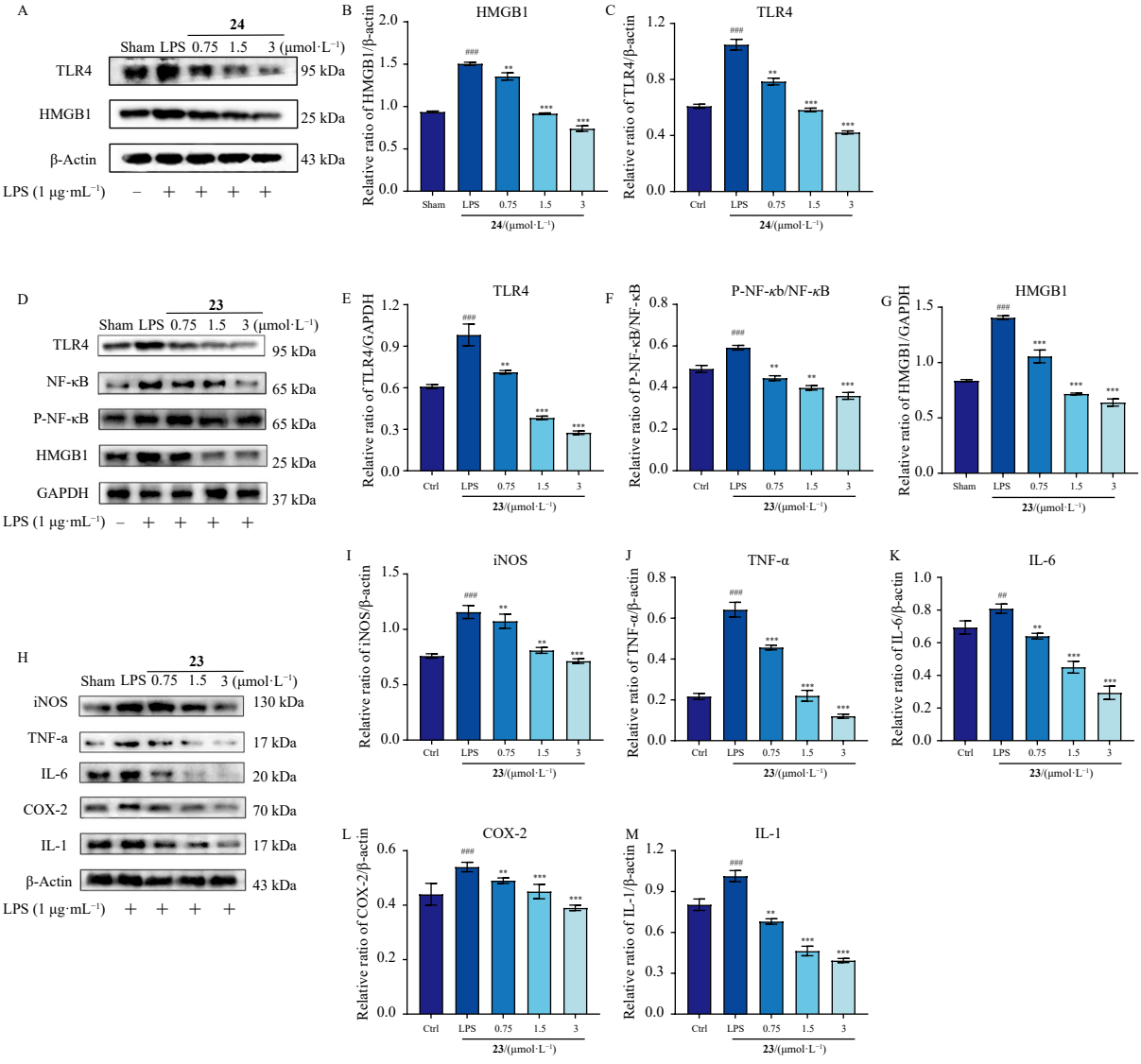


Fig. 16 Effects of compound **23** and **24** on inflammatory factors in RAW264.7 cells. (A), (D) and (H) are results of Western blotting, GAPDH and β-actin as an internal reference; (B) and (C) represent the effects of compound 24 on the relative expression levels of TLR4 and HMGB1 proteins, respectively; (E), (F), (G), (I), (J), (K), (L), and (M) represent the effects of compound 23 on the levels of TLR4, NF-κB, HMGB1, iNOS, TNF-α, IL-6, COX-2, and IL-1 proteins, respectively. Data are presented as mean ± SD (n = 3 independent tests). $^{*}P < 0.05$, $^{**}P < 0.01$, $^{***}P < 0.001$ *vs* the LPS group; $^{\#\#}P < 0.01$, $^{\#\#\#}P < 0.001$ *vs* the blank control group.

way, as the downstream effector of RAGE, showed a significant decrease in the phosphorylation level of these two key signaling molecules. Therefore, the compounds inhibited inflammation stress by blocking HMGB1/TLR4/NF-κB and HMGB1/RAGE signaling pathway and downregulating the expression of PI3K/AKT pathway-related proteins. This effect promotes the cells apoptosis.

In summary, we draw a conclusion the compounds take strong anti-colorectal cells proliferation effects by both anti-inflammation and promoting apoptosis.

2.9. Therapeutic effect of compound in CT26.WT mouse model

To determine the acute toxicity of the compound *in vivo* and the dose to be administered in animal bioactivity studies, the LD_{50} value was first predicted by intraperitoneal injection of compound **23** (high, medium and low dose groups) into 6-week-old BALB/c mice (male and female, n = 5 per group). In the 1000 mg·kg^{-1} dose group, three mice died from day 1 onward, while the remaining mice experienced rapid weight loss. All mice in the group died within 14 days, indicating that compound **23** at this dose exhibited high toxicity. As for the 300 mg·kg^{-1} dose group, all the mice showed sustained weight gain and no one died within 14 days, suggesting compound **23** had a lower toxicity at this dosage. While in the 600 mg·kg^{-1} dose group, the mice continuously weighted loss from day 1 to day 4, followed by gradual weight recovery after day 4; finally, two mice died on days 2 and one on days 3 post-administration, with in total three mice died within 14 days. This indicates that compound **23** at the 600 mg·kg^{-1} dose showed some toxicity in some degree, and half of the mice died, suggesting that the half number lethal dose (LD_{50}) of compound **23** should be approximately 600 mg·kg^{-1}.

To further assess the therapeutic effect of the compound *in vivo*, the CT26.WT mouse colon cancer cells were subcutaneously injected into Balb/c mice to model the tumor. When the tumor size reached about 100 mm^3, the mice were divided into four groups, model control group, positive control group, low-dose group and high-dose group. The mice was administered by intraperitoneal injection once daily, with 5-FU as the positive control; PBS was administered in the model group. Meanwhile, the tumor growth was monitored for about 14 days. As shown in Fig. 18, for both the compounds groups and 5-FU group, the tumor size and body weight significantly reduced compared to that in the model group; moreover, for the compounds groups, the tu-

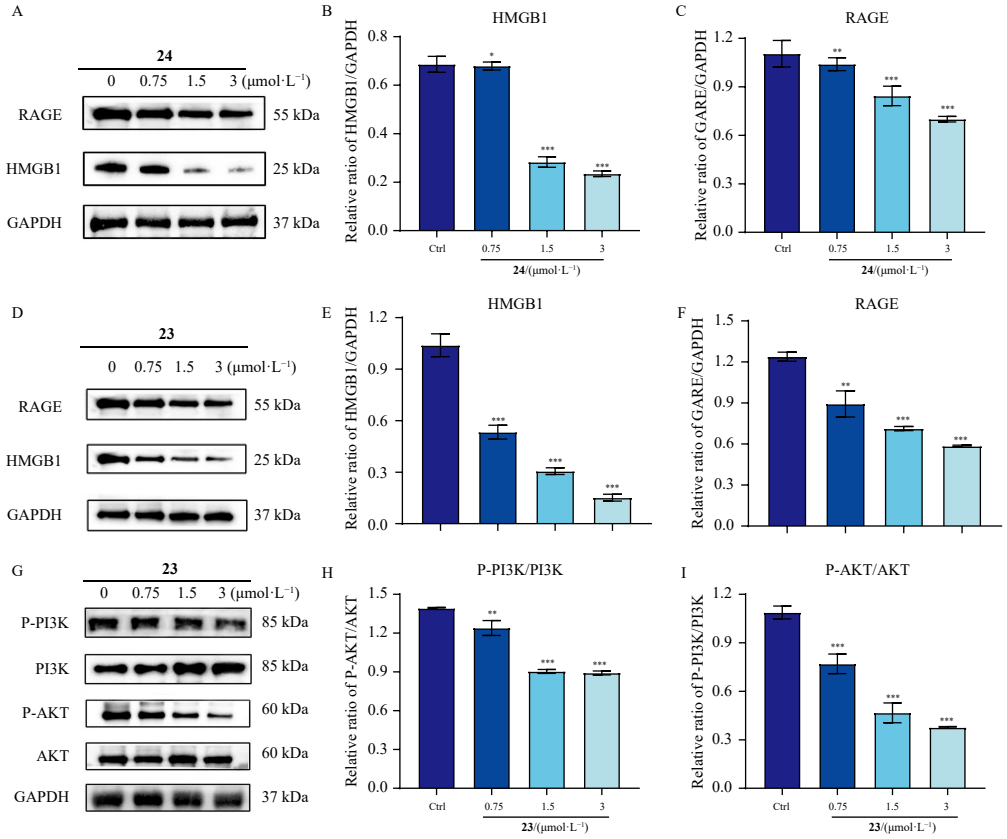


Fig. 17 Effects of compound **23** and **24** on the expression of proteins related to HMGB1/RAGE pathway; and effects of compound **23** on the expression of proteins related to PI3K/AKT pathway. (A, D, G) The results of Western blotting, with GAPDH as the internal control. (B, C) The effects of compound **24** on the relative expression levels of HMGB1 and RAGE proteins, respectively. (E–I) The effects of compound **23** on the relative expression levels of HMGB1, RAGE, PI3K, and AKT proteins. Data are presented as mean ± SD (n = 3 independent tests). $^{*}P < 0.05$, $^{**}P < 0.01$, $^{***}P < 0.001$ *vs* the compound group and the blank control group.

mors were smaller and the body weights were lower than those of 5-FU group, and it was dose-dependent. Among them, compound **23** demonstrated a superior efficacy compared to compound **24**. This indicates that compounds have a good colorectal cancer therapeutic effect, and it is much stronger than 5-FU at the same doses. This is consistent with results from *in vitro* studies.

To show the therapeutic effect of compounds **23** and **24** is related to anti-inflammation, the expression levels of inflammatory factors HMGB1, TNF-α and IL-6 in mouse serum were measured by ELISA. As shown in Figs. 19A and 19B, when compound **23** was 30 mg·kg^{-1}, the expression levels of HMGB1 and RAGE in serum of colon cancer model mice were reduced to 56.41% and 58.28% of the model control group; for **24**, the expression levels of HMGB1 and RAGE decreased to 65.38% and 70.54% of that, respectively; Meanwhile, the expression levels of TNF-α and IL-6 in serum decreased in a dose-dependent manner; compared with 5-FU, it still showed stronger activities (Figs. 19C and 19D). In contrast, compound **23** has a better activity than compound **24**. This indicates that both the compounds inhibited the proliferation and development of colon cancer, at least partly mechanism is achieved by reducing inflammation in colon cancer tissues. This is consistent with in vitro results.

3. Conclusions

Colorectal cancer is a highly immune-related disease, and its TME determines its cells survival and development. Severe inflammation in TME prevents immune cells to play a role, and the barrier effect of TME makes drugs difficult to distribute into the tumor cells. To obtain the compounds which both having strong inflammatory activities in TME and inhibiting the proliferation of colorectal cancer cells, GN derivatives based on HMGB1 as the target were synthesized and evaluated. CCK-8 results showed that all compounds had inhibition on the cell proliferation in some degree. Of them, compound **22** with two hydroxyl groups in cassia bark acid aryl ring showed the strongest activity against HCT116 colon cancer cells (IC_{50} 13.1 μmol·L^{-1}) among them; however, its water solubility is poor. To enhance the solubility of compound, compound **23** and **24** were screened among compounds **23**–**40**. They displayed strong activity against CT26 cells, with IC_{50} value 1.1 and 1.4 μmol·L^{-1}. This indicates both compounds have strong selective inhibition to colon cancer CT26 cells. Possibly the guanidine group at C30 position enhanced the proliferative inhibition on CT26 cells. In following tests, the compounds also showed a strong anti-proliferative activity against CT26 cells, and it was far stronger than the positive control 5-FU and GA. Secondly, they blocked CT26 cells in G_2/M phase and blocked cell cycle and promoted apoptosis, and it was concentration-dependent; meanwhile, both compounds downregulated the expression levels of Bcl-2 and MMP-9 in a concentration dependent manner. Western Blot analysis revealed the levels of cyclin B1 and CDK1 also decreased in a concentration-dependent manner. Besides that, the cyclin A2 level also downregulated, suggesting the compounds simultaneously blocked the progression from S phase to G_2 phase, leading to cellular arrest at the G_2/M stage.

In the anti-inflammatory tests, compound **23** was able to reduce the levels of inflammatory factors in both RAW264.7 cells and CT26 colon cancer cells, and the IC_{50} values were 10.3 and 1.1 μmol·L^{-1} against NO production, respectively. In addition to NO, compound **23** suppressed the persistence and amplification of inflammatory responses by reducing intracellular ROS levels and increasing MMP. Western Blot showed, after treatment of CT26 cells with **23**, the levels of TLR4 and HMGB1 decreased in a concentration-dependent manner, and the phosphorylation of NF-κB p65 was inhibited; correspondingly, TNF-α, IL-6, IL-1 and COX-2 levels also decreased in a concentration-dependent manner. In

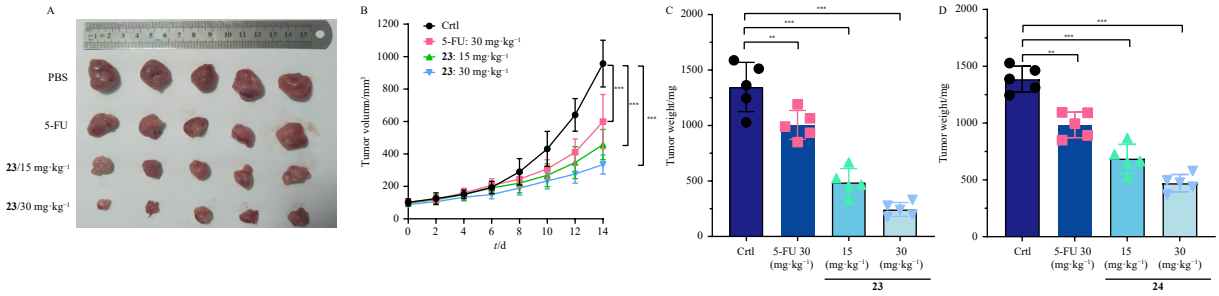


Fig. 18 Effects of compound on tumor volume and weight in Balb/c Mice (5-FU, positive control). Tumor images (A), tumor volume (B), and tumor weight (C) after treatment with compound **23**, respectively. (D) Tumor weight after treatment with compound **24**. Data are presented as mean ± SD (n = 5 independent tests). $^{*}P < 0.05$, $^{**}P < 0.01$, $^{***}P < 0.001$ *vs* blank control group.

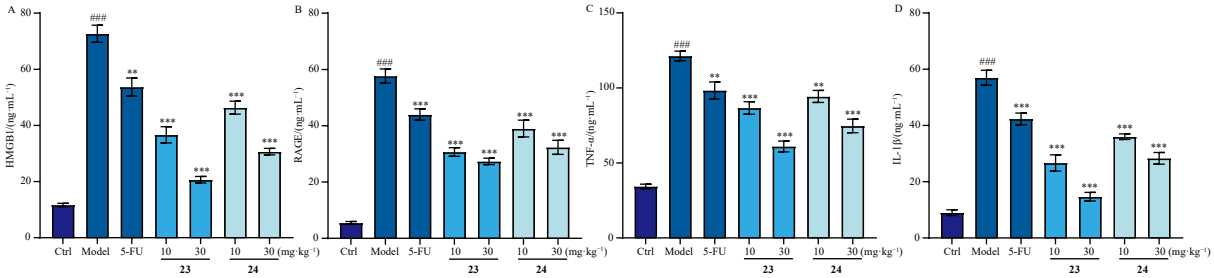


Fig. 19 Effects of compounds **23** and **24** on serum levels of HMGB1 (A), RAGE (B), IL-1β (C), and TNF-α (D) in a colon cancer mouse model (5-FU, positive control). Data are presented as mean ± SD (n = 3 independent tests). $^{*}P < 0.05$, $^{**}P < 0.01$, $^{***}P < 0.001$ *vs* the Model group; $^{\#\#\#}P < 0.001$ *vs* the blank control group.

addition, compound **23** also blocked the HMGB1/RAGE signal pathway and downregulated the expression levels of PI3K/AKT pathway related proteins, thereby inhibiting the proliferation of CT26 cells. Therefore, compound **23** not only has good anti-inflammation activity, but also can inhibit CT26 cells proliferation, and it is one of compounds we hope to seek.

Especially, in animal tests, compounds **23** and **24** reduced in tumor size and body weight in dose-dependent manner, and it was more significant than the positive control 5-FU. Moreover they decreased the levels of HMGB1, RAGE, IL-6 and TNF-α, this indicates their anticancer activity is consistent the anti-inflammation activity. In contrast, compound **23** is better.

In conclusion, through design and structural modification and screening, compound **23** with dual inhibitory effects on cancer cell proliferation were obtained. It not only strongly inhibited the proliferation of colon cancer cells (CT26), but also showed a strong anti-inflammatory activity in the tumor microenvironment. Therefore, compound **23** will be a great potential as a candidate drug for anti-colorectal cancer therapy, and deserve to further investigate.

4. Experimental

4.1. Materials and instruments

All details see Supplementary materials.

4.2. Synthesis of the compounds

All details see Supplementary materials.

4.3. Cell experiments

A549, Huh7, CT26, Hela, HCT116, HT-29, and HEPG-2 cells were cultured and passaged in high-glucose DMEM (HyClone) medium supplemented with heat-inactivated fetal bovine serum (10%) and antibiotics penicillin/streptomycin (1%). SK-HEP-1 cells were cultured and passaged in 1640 medium supplemented with 10% fetal bovine serum and 1% antibiotics (penicillin/streptomycin). RAW264.7 cells were cultured and passaged in DMEM medium supplemented with 10% fetal bovine serum and 1% antibiotic (penicillin/streptomycin). All culture conditions were maintained at 37 °C, 5% CO_2, and 95% humidity.

4.3.1. Compound cytotoxicity assessment

Seed the cell suspension into a 96-well plate (5 × 10^3 cells per well) for 24 h, then add 10 μL of CCK-8 solution to each well and continue incubating the cells in the incubator for 1–4 h. Measure the absorbance values of each well at a wavelength of 450 nm using an enzyme-linked immunosorbent assay (ELISA) reader, calculate the IC_{50} of each compound, and use it to indicate the effect of each drug on cell survival rate.

4.3.2. EDU cell proliferation assay

Cells were seeded into a 96-well plate (6 × 10^3 cells/well) and incubated overnight. After treating with various concentrations of the test compound for 24 h, EdU staining solution was added, and the cells were incubated at 37 °C for 2 h. After 2 h, the cells were fixed with 3.7% paraformaldehyde for 15 min and washed three times with BSA. After centrifugation, add Triton X-100 and incubate for 20 min. Then add the fluorescent dye and incubate in the dark for 30 min, followed by washing the cells with BSA. Subsequently, stain the nuclei with DAPI and observe under a fluorescence microscope. Finally, count the EdU-positive cells using ImageJ software (NIH, Bethesda, MD).

4.3.3. Cell cloning experiment

Disperse the cells in 3 mL of the corresponding medium containing serum, and inoculate the suspension into a six-well plate (1–2 × 10^3 cells/well). Treat the cells with a specific concentration of the compound for 1–2 weeks until colonies form, replenishing the medium every 3 days during this period. After the cloning experiment, gently wash the cell colonies twice with PBS, fix them with 4% (*W*/*V*) paraformaldehyde for 10 min, and finally stain them with 1% crystal violet for 15 min. Photograph the colonies using an optical microscope (Moticam Pro282B) and count the number of colonies.

4.3.4. Cell cycle experiment

Cells in the logarithmic growth phase (4.5 × 10^5 cells/well) were seeded into a 6-well plate for culture. After the cells have adhered, treat them with different concentrations of the compound for 24 h. Then digest and collect the cells with trypsin, wash them twice with PBS buffer pre-cooled to 4 °C, and fix the cells with 70% ethanol solution pre-cooled to 4 °C for 12 h according to the kit instructions. Subsequently, stain the cells with PI dye for 30 min and perform cell cycle analysis using a flow cytometer.

4.3.5. cell scratch assay

Add the cell suspension to a 6-well plate. After the cells have adhered, observe under an optical microscope to confirm that the cells completely cover the bottom surface of each well. Use the tip of a 10 μL sterile pipette to draw three straight lines in each well. Subsequently, add different concentrations of the test compounds and capture images of the same scratch area at 0, 24, and 48 h. The scratch area is calculated using Image*J* software.

4.3.6. Hoechst and Giemsa staining experiments

Seed cells at a density of 4000 cells per well in a 6-well plate. After the cells have adhered, add the test compounds at different concentrations. After incubation for 24 , remove the supernatant, fix the cells with 4% (*W*/*V*) paraformaldehyde for 30 min, then add Giemsa or Hoechst 33342 staining solution diluted tenfold with deionized water, and stain the cells for 30 min. Finally, rinse off the excess dye with deionized water, observe the cell morphology under an optical microscope, and take photographs.

4.3.7. Apoptosis assay

Seed the cell suspension (3 × 10^5 cells/well) into a 6-well plate. After the cells have adhered, add the test compounds at different concentrations. After 24 h, collect the cells by trypsin digestion, rinse with pre-chilled PBS (4 °C), and resuspend in 100 μL of 1 × Binding Buffer. Add 5 μL of Annexin V-FITC and 10 μL of PI staining solution to the sample. After staining in the dark for 15 min, add 400 μL of 1 × Binding Buffer. Finally, analyze the sample using a flow cytometer.

4.3.8. Mitochondrial membrane potential (MMP) change detection experiment

Seed cells (3 × 10^5 cells/well) into a 6-well plate. After the cells have adhered, add different concentrations of the test compound and incubate for 24 h. Collect the cells through digestion and centrifugation, then incubate the cells with a 100 nmol·L^{-1} TMRE solution for 30 min. After incubation, wash the cells with PBS. Subsequently, use a flow cytometer to detect the effect of the compound on the mitochondrial membrane potential of the cells.

4.3.9. Reactive oxygen species (ROS) burst detection experiment

Cultivate cells in a 6-well plate (3 × 10^5 cells/well). After the cells adhered, add different concentrations of the test compound and continue incubation. After 24 h of incubation, collect the cells by trypsin digestion, wash once with PBS, then add a DCFH-DA solution diluted with culture medium to the sample and incubate the cells for 30 min. Wash the cells with PBS and use a flow cytometer to detect the effect of the compound on ROS.

4.3.10. Protein immunoblotting

Cultivate cells in a 6-well plate (3 × 10^5 cells/well). After 24 h, add the test compound and set up DMSO control wells. After the compound has acted for 24 h, remove the supernatant, wash with PBS, add pre-chilled lysis buffer, and lyse on ice at 4 °C. After 15 min, centrifuge at 12 000 r·min^{-1}. After 15 min, perform BCA protein quantification, then add protein loading buffer for denaturation. Prepare the gel according to the kit instructions, load 30 μg of protein per group, and run at 80 V constant voltage for 30 min under ice bath conditions until the samples are on the same line. Switch to 120 V constant voltage and run for 60 min. Install the membrane transfer clamp and perform membrane transfer at a constant current of 200 mA for 60 min to transfer the proteins to the PVDF membrane. Block the PVDF membrane for 120 min, wash with TBST, cut out the bands, and incubate overnight at 4 °C with the corresponding primary antibody. Wash with TBST and incubate in the corresponding secondary antibody on a shaking incubator. After 90 min, wash with TBST. Add ECL chemiluminescent solution, detect using a chemiluminescence detector, and analyze data using ImageJ.

4.3.11. Effect of compounds on NO release levels

Seed RAW264.7 cell suspension into a 96-well plate. After the cells have adhered, divide them into a blank group, an LPS group, and an LPS + compound group. After 24 h of cell culture, 50 μL of supernatant was transferred to a new 96-well plate according to the Griess reagent kit instructions. 50 μL of Griess reagent A and 50 μL of Griess reagent B were added sequentially, and the mixture was incubated at room temperature for 5 minutes. The absorbance values at 540 nm were measured using a microplate reader, and the IC_{50} values for each compound were calculated.

4.4. Establishment of a subcutaneous tumor model in mice and evaluation of compound effects

Subcutaneous injection of 2 × 10^6 CT26 cells was performed to establish a subcutaneous CT26 tumor mouse model. On day 10, the tumor volume in Balb/c mice was approximately 70 mm^3, and the mice were randomly divided into 4 groups (n = 5). The mice were then administered saline, 5-FU (30 mg·kg^{-1}), or compound **23** (15, 30 mg·kg^{-1}) *via* intravenous injection once daily for 14 d. Tumor volume was measured using calipers, calculated using the formula: Tumor volume = (tumor length × tumor $width^2$)/2. Body weight and tumor volume were recorded every 2 days for each group of mice. After 14 d of treatment, mice in each group were euthanized,

Supplementary materials

Supplementary materials can be requested by sending E-mail to the corresponding authors.

Declaration of competing interest

These authors have no conflict of interest to declare.

References

1 Walle GT, Kitaw TA, Adane S. Incidence and determinants of mortality among patients with colorectal cancer in oncology centers of Amhara region, Ethiopia, 2024: multicenter retrospective follow up study. *BMC Cancer*. 2025;25(1):102. https://doi.org/10.1186/s12885-025-13462-z.

2 Lourenço FC, Sadien ID, Wong K, et al. Decay of driver mutations shapes the landscape of intestinal transformation. *Nature*. 2026;649(8097):729-738. https://doi.org/10.1038/s41586-025-09762-w.

3 Sung HYA, Siegel RL, Laversanne M, et al. Colorectal cancer incidence trends in younger versus older adults: an analysis of population-based cancer registry data. *Lancet Oncol*. 2025;26(1):51-63. https://doi.org/10.1016/S1470-2045(24)00600-4.

4 Dekker E, Tanis PJ, Vleugels JLA, et al. Colorectal cancer. *Lancet*. 2019;394(10207):1467-1480. https://doi.org/10.1016/S0140-6736(19)32319-0.

5 Gray R, Hills R, Stowe R, et al. Adjuvant radiotherapy for rectal cancer: a systematic overview of 8507 patients from 22 randomised trials. *Lancet*. 2001;358(9290):1291-1304. https://doi.org/10.1016/S0140-6736(01)06409-1.

6 Chai Y, Liu JL, Zhang S, et al. The effective combination therapies with irinotecan for colorectal cancer. *Front Pharmacol*. 2024;15:1356708. https://doi.org/10.3389/fphar.2024.1356708.

7 Barriuso J, Nagaraju RT, Belgamwar S, et al. Early adaptation of colorectal cancer cells to the peritoneal cavity is associated with activation of "sternness" programs and local inflammation. *Clin Cancer Res*. 2021;27(4):

1119-1130. https://doi.org/10.1158/1078-0432.CCR-20-3320.
8 Xia W, Geng YT, Hu WW. Peritoneal metastasis: a dilemma and challenge in the treatment of metastatic colorectal cancer. *Cancers*. 2023;15(23): 15235641. https://doi.org/10.3390/cancers15235641.
9 Liu WX, Kuang TR, Liu L, et al. The role of innate immune cells in the colorectal cancer tumor microenvironment and advances in anti-tumor therapy research. *Front Immunol*. 2024;15:1407449. https://doi.org/10.3389/fimmu.2024.1407449.
10 Ganesh K, Stadler ZK, Cercek A, et al. Immunotherapy in colorectal cancer: rationale, challenges and potential. *Nat Rev Gastroenterol Hepatol*. 2019;16 (6):361-375. https://doi.org/10.1038/s41575-019-0126-x.
11 Schmitt M, Greten FR. The inflammatory pathogenesis of colorectal cancer. *Nat Rev Immunol*. 2021;21(10):653-667. https://doi.org/10.1038/s41577-021-00534-x.
12 Wang H, Tian T, Zhang JH. Tumor-associated macrophages (TAMs) in colorectal cancer (CRC): from mechanism to therapy and prognosis. *Int J Mol Sci*. 2021;22(16):8470. https://doi.org/10.3390/ijms22168470.
13 Shah SC, Itzkowitz SH. Colorectal cancer in inflammatory bowel disease: mechanisms and management. *Gastroenterology*. 2022;162(3):715-730.e713. https://doi.org/10.1053/j.gastro.2021.10.035.
14 Wang SM, Zhang Y. HMGB1 in inflammation and cancer. *J Hematol Oncol*. 2020;13(1):116. https://doi.org/10.1186/s13045-020-00950-x.
15 Schiraldi M, Raucci A, Muñoz LM, et al. HMGB1 promotes recruitment of inflammatory cells to damaged tissues by forming a complex with CXCL12 and signaling *via* CXCR4. *J Exp Med*. 2012;209(3):551-563. https://doi.org/10.1084/jem.20111739.
16 Chen RC, Kang R, Tang DL. The mechanism of HMGB1 secretion and release. *Exp Mol Med*. 2022;54(2):91-102. https://doi.org/10.1038/s12276-022-00736-w.
17 Yang H, Antoine DJ, Andersson U, et al. The many faces of HMGB1: molecular structure-functional activity in inflammation, apoptosis, and chemotaxis. *J Leukoc Biol*. 2013;93(6):865-873. https://doi.org/10.1189/jlb.1212662.
18 Wang YY , Yu ZM, Yuan H, et al. Structure-based design of glycyrrhetinic acid derivatives as potent anti-sepsis agents targeting high-mobility group box-1. *Bioorg Chem*. 2021;106:104461. https://doi.org/10.1016/j.bioorg.2020.104461.
19 Qiang X, Peng YJ, Wang ZY, et al. Synthesis of glycyrrhizin analogues as HMGB1 inhibitors and their activity against sepsis in acute kidney injury. *Eur J Med Chem*. 2023;259:115696. https://doi.org/10.1016/j.ejmech.2023.115696.
20 Zhang QP, Wang YN, Wang ZY, et al. Synthesis and anti-inflammatory activities of glycyrrhetinic acid derivatives containing disulfide bond. *Bioorg Chem*. 2022;119:105542. https://doi.org/10.1016/j.bioorg.2021.105542.
21 Martin Sahn AG, Lucie Heller,Wajid Hussain, et al. Synthesis and cytotoxicity of 3-amino-glycyrrhetinic acid derivatives. *Mediterr J Chem*. 2018;7(1):39-55. https://doi.org/10.13171/mjc71/01804111430-cesuk.
22 Wang R, Yang W, Fan YQ, et al. Design and synthesis of the novel oleanolic acid-cinnamic acid ester derivatives and glycyrrhetinic acid-cinnamic acid ester derivatives with cytotoxic properties. *Bioorg Chem*. 2019;88:102951. https://doi.org/10.1016/j.bioorg.2019.102951.
23 Xu Q, Deng H, Li XT, et al. Application of amino acids in the structural modification of natural products: a review. *Front Chem*. 2021;9:650569. https://doi.org/10.3389/fchem.2021.650569.
24 Cui HW, He Y, Wang J, et al. Synthesis of heterocycle-modified betulinic acid derivatives as antitumor agents. *Eur J Med Chem*. 2015;95:240-248. https://doi.org/10.1016/j.ejmech.2015.03.048.
25 Zhang CZ, Yan WQ, Zhao R, et al. Design, synthesis and evaluation of new ligustrazine derivatives as potential plasma-stable neuroprotective agents. *Medchemcomm*. 2017;8(3):652-656. https://doi.org/10.1039/c7md00003k.
26 Falbo F, Gemma S, Koch A, et al. Synthetic derivatives of natural cinnamic acids as potential anti-colorectal cancer agents. *Chem Biol Drug Des*. 2024; 103(1):e14415. https://doi.org/10.1111/cbdd.14415.
27 Cabello CM, Bair III WB, Lamore SD, et al. The cinnamon-derived Michael acceptor cinnamic aldehyde impairs melanoma cell proliferation, invasiveness, and tumor growth. *Free Radic Biol Med*. 2009;46(2):220-231. https://doi.org/10.1016/j.freeradbiomed.2008.10.025.
28 He R, Dong T, Chu J, et al. Phaser-trim: a phase separation based genetically encoded reporter for H3K9 trimethylation in living cells. *Anal Chem*. 2024;96 (32):13007-13014. https://doi.org/10.1021/acs.analchem.4c00992.
29 Jiang M, Qi F, Zhang K, et al. MARCKSL1-2 reverses docetaxel-resistance of lung adenocarcinoma cells by recruiting SUZ12 to suppress HDAC1 and elevate miR-200b. *Mol Cancer*. 2022;21(1):150. https://doi.org/10.1186/s12943-022-01605-w.
30 Barcia JJ. The Giemsa stain: its history and applications. *Int J Surg Pathol*. 2007;15(3):292-296. https://doi.org/10.1177/1066896907302239.
31 Crowley LC, Marfell BJ, Waterhouse NJ. Analyzing cell death by nuclear staining with Hoechst 33342. *Cold Spring Harb Protoc*. 2016;2016(9):087205. https://doi.org/10.1101/pdb.prot087205.
32 Ragonese F, Monarca L, De Luca A, et al. Resveratrol depolarizes the membrane potential in human granulosa cells and promotes mitochondrial biogenesis. *Fertil Steril*. 2021;115(4):1063-1073. https://doi.org/10.1016/j.fertnstert.2020.08.016.
33 Trachootham D, Alexandre J, Huang P. Targeting cancer cells by ROS-mediated mechanisms: a radical therapeutic approach? *Nat Rev Drug Discov*. 2009;8(7):579-591. https://doi.org/10.1038/nrd2803.
34 Carneiro BA, El-Deiry WS. Targeting apoptosis in cancer therapy. *Nat Rev Clin Oncol*. 2020;17(7):395-417. https://doi.org/10.1038/s41571-020-0341-y.
35 Xu X, Piao HN, Aosai F, et al. Arctigenin protects against depression by inhibiting microglial activation and neuroinflammation *via* HMGB1/TLR4/NF-κB and TNF-α/TNFR1/NF-κB pathways. *Br J Pharmacol*. 2020;177(22): 5224-5245. https://doi.org/10.1111/bph.15261.
36 van Beijnum JR, Buurman WA, Griffioen AW. Convergence and amplification of toll-like receptor (TLR) and receptor for advanced glycation end products (RAGE) signaling pathways *via* high mobility group B1 (HMGB1). *Angiogenesis*. 2008;11(1):91-99. https://doi.org/10.1007/s10456-008-9093-5.